AN ABSTRACT OF THE THESIS OF

Richard D. Lutz, Jr. for the degree of Master of Science in

Electrical and Computer Engineering presented on June 3rd, 1998.

Title:

Analysis and Modeling of Planar Microstrip Spiral Inductors on Lossy Substrates.

Abstract approved: Redacted for Privacy

Vijai K. Tripathi

The advent of low-cost RFIC's fabricated in Silicon-based technologies has led to the use of monolithic lumped elements which are located on-die. While it is clearly advantageous to have a high degree of integration and thus fewer off-chip elements, parasitic losses due to semiconducting substrate effects can be a performance-limiting factor. Microstrip spiral inductors are key components in many high frequency circuit designs, including MMIC's, RFIC's, and mixed-signal modules. However, the losses associated with spirals fabricated in a lossy substrate environment, such as in CMOS and bipolar technologies, are not accurately modeled by the current conventional techniques. This thesis presents a complete modeling technique for spiral inductors over such 'high-loss' substrates.

The quasi-static solution for single and coupled Metal-Insulator-Substrate (MIS) microstrip structures has led to the development of methods for calculating the self and mutual line parameters r, l, g, and c, which are in turn utilized in the model for the microstrip spiral inductors in the same environment. The equivalent circuit model for the spiral inductors is based on the conventional low-loss spiral models with the inclusion of frequency-dependent losses due to semiconducting

substrates. The distributed model for spirals in CMOS-based RFICs incorporates inductance calculations by the Partial Element Equivalent Circuit (PEEC) method, augmented by inductance and resistance calculations for the so-called skin effect mode by the spectral domain technique. In addition, the capacitances and shunt conductances can be computed by a Poisson solver for layered lossy media; both network analog and spectral domain methods are also used to find the shunt admittance per unit length for the microstrip structure as a fundamental element of the spiral. Simulations for typical structures have been performed to validate the modeling techniques via comparison with a commercial simulator and network analyzer measurements for a 9.5 turn spiral in CMOS for RFIC applications.

Analysis and Modeling of Planar Microstrip Spiral Inductors on Lossy Substrates

by

Richard D. Lutz, Jr.

A THESIS

submitted to

Oregon State University

in partial fulfillment of
the requirements for the
degree of

Master of Science

Completed June 3rd, 1998
Commencement June 1999

Master of Science thesis of Richard D. Lutz, Jr. presented on June 3rd, 1998

APPROVED:

Redacted for Privacy

Major Professor, representing Electrical and Computer Engineering

Redacted for Privacy

Chair of the Department of Electrical and Computer Engineering

Redacted for Privacy

Dean of the Graduate School

I understand that my thesis will become part of the permanent collection of Oregon State University libraries. My signature below authorizes release of my thesis to any reader upon request.

Redacted for Privacy

Richard D. Lutz, Jr., Author

ACKNOWLEDGMENTS

First I wish to thank my major professor, Dr. Vijai K. Tripathi, for providing me with the opportunity to do great research work with him and for giving constant support and encouragement during my years in graduate school.

I would also like to thank Dr. Andreas Weisshaar, my minor professor, who has been available for many useful discussions on my work and has been a great source of support as well.

Thanks is due to Dr. Tom Plant and Graduate Council Representative Dr. Bruce D'Ambrosio for serving on my graduate committee and reviewing the manuscript.

I also thank my colleagues, Alok Tripathi, Ed Godshalk, Dr. Maynard Falconer, Jeff Williams, Kate Remley, and Yeon-Chang Hahm for their encouragement, useful discussions, and contributions to this work.

Thanks to Aiko Kobayashi for her understanding and support during my graduate studies.

Finally, many thanks to the International Microelectronics and Packaging Society for awarding me an Educational Foundation Grant for the 1996-1997 academic year, and to Intel Corporation, Hewlett Packard Company, and the Electrical and Computer Engineering Department at Oregon State University for their financial and academic support.

TABLE OF CONTENTS

TABLE OF CONTENTS (Continued)

LIST OF FIGURES

LIST OF FIGURES (Continued)

LIST OF FIGURES (Continued)

DEDICATION

This thesis is dedicated to the memory of my parents, Richard and Dorothy Lutz, who provided me with the guidance, love and support for me to to be successful in my educational endeavours as well as life in general.

ANALYSIS AND MODELING OF PLANAR MICROSTRIP SPIRAL INDUCTORS ON LOSSY SUBSTRATES

1. INTRODUCTION

Inductance is a measure of magnetic flux linkage per unit current, and consequently magnetic energy storage circuit elements are known as inductors. Such inductive elements come in a variety of shapes and sizes, ranging from toroids and solenoids for relatively large scale circuits, to monolithic structures for use in integrated circuits. A primary example of the latter is a planar microstrip spiral inductor which is an integral part of many radio frequency (RF) and microwave frequency circuit designs, as the realizable inductances of such structures are, in general, appropriate for the design frequency ranges of interest.

RF integrated circuits (RFICs) are being increasingly fabricated in silicon technology, including CMOS, as a means of cost reduction. The use of spiral inductors in RFICs has created a need for accurate models of these structures in the lossy substrate environments which are typical for many silicon-based processes. The existing CAD-oriented modeling techniques for microstrip spiral inductors above low-loss substrates [1, 2] are not accurate when substrate conductivities are on the order of 10^4 S/m and isolation from the semiconducting substrate is minimal, as is typical for a CMOS environment. The primary reason that the low-loss models are not sufficient is that the effects of magnetic fields in the semiconducting substrate and resultant currents produce considerable degrading effects and can limit a spiral's performance.

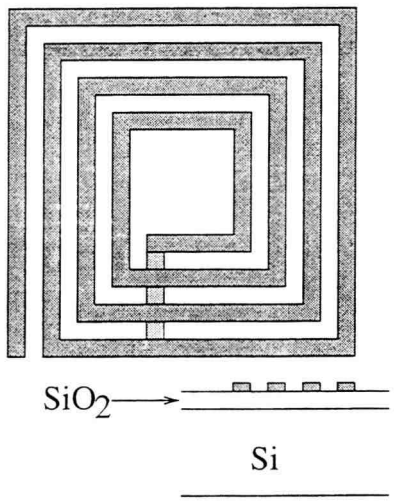

FIGURE 1.1. Example of a Si-SiO_2-based spiral structure

This thesis presents a comprehensive analysis and design methodology for spiral inductor structures in lossy media primarily for RF applications. An example structure of a spiral in a Si-SiO_2 environment is shown in Figure 1.1 . The techniques for modeling lossless structures are augmented via inclusion of appropriate loss mechanisms including radiation and conduction currents in the semiconducting substrate regions. One resounding theme throughout this thesis with regard to inductance calculations is the concept of partial inductance which is reviewed in Appendix A.

Chapter Two presents a general modeling methodology for single and multilevel spirals in low loss media. The inductance formulae used in this work are those of Greenhouse [3], who authored a now heavily referenced paper on a simple algorithm to estimate the inductance of planar rectangular spirals. The frequency dependence of the spiral inductors brought about by parasitic reactances and conductor and substrate losses are also included.

Chapter Three describes the loss mechanisms for microstrip structures above semiconducting substrates as is typical in a CMOS or bipolar process. The modeling techniques for spiral inductors in such environments are based on analysis of microstrip as a fundamental element of the structures. The losses associated with microstrip structures over semiconducting substrates have been addressed in many publications including [4–6]. This chapter presents a complete modeling methodology that incorporates lumped equivalent circuits for microstrip and spirals. A modified Spectral Domain Approach (SDA) using complex dielectric constants is used in the computation of capacitances and shunt/transverse conductances. It is also shown that a circuit topology based on the physical nature of the structure may be employed to represent the frequency dependent behavior of these capacitances and conductances. The concept of Partial Element Equivalent Circuits (PEEC), which was first developed by Ruehli [19] in 1974, is introduced for highly accurate inductance calculations. Sensitivity analysis on the accuracy of different inductance calculation methods is also performed.

Chapter Four examines the effects on performance caused by varying certain design parameters for typical spirals and describes the model validation. The effects of varying parameters including substrate conductivity and oxide height are analyzed to provide general design rules for spirals in a high loss environment.

Chapter Five contains conclusions and suggestions for future work.

2. SPIRAL INDUCTORS IN LOW LOSS MEDIA

2.1. Introduction

Analysis of inductors in low loss media is an appropriate area for gaining insight into the general behavior of spiral inductors. This chapter deals with the design considerations and modeling techniques for low-loss single and multilevel spirals.

An example of a typical single level spiral is shown in Figure 2.1. As a lossless dielectric substrate is assumed here, there are only inductances and capacitances to be considered for an analysis and modeling effort. The following section is concerned primarily with multilevel and multilayer spiral designs, but the techniques described are applicable to any inductor in a lossless medium.

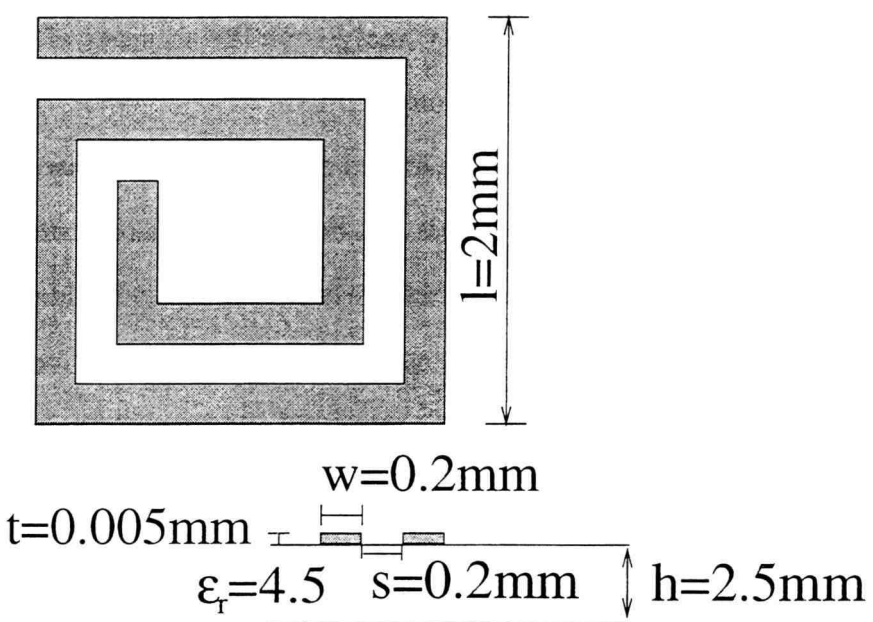

FIGURE 2.1. Schematic of an example rectangular spiral

2.2. Multilayer Inductors

Spiral inductors embedded in multilayered media offer an attractive solution to the implementation of such off-chip lumped elements in RF and mixed signal circuits. Design issues to be considered for these structures include the inductance values, quality factor, electromagnetic interference (EMI), and the frequency range of operation.

The quality factor, Q, for a spiral inductor is influenced by losses that include dielectric, radiation and conductor losses. The substrate loss is an important limiting factor in designing on-chip spirals on Si-based ICs such as CMOS RFICs.

Modeling and design techniques for spiral inductors include lumped element equivalent circuit models [1], distributed coupled line models [7–9], or full wave simulation [10]. While the last method yields the greatest accuracy for a design, it is also computationally taxing, and often a simpler CAD oriented model will suffice for given fabrication and material tolerances.

Closed form expressions for self and mutual inductances of both straight planar conductor segments and circular structures have been presented in [1, 3, 11]. These expressions lead to an accurate estimate of the static inductance for given structural geometry with or without a ground plane. For a complete model of the spiral inductor distributed capacitances, losses due to finite conductivity of the spiral metallization, and dielectric substrate losses must also be included.

The radiation analysis for a structure yields additional loss terms in the model as well as field expressions which may be used to model coupling of the spiral with other components in the far zone. In addition, near-field inductive terms can be used to calculate coupling between elements in close proximity.

2.3. Design Considerations for Single and Multilayer Spirals

When considering an inductor structure, parameters such as quality factor and self resonant frequency, ω_o, are key design issues. A maximum usable frequency range and minimization of losses are both desirable qualities for an inductor, and thus CAD oriented models which can accurately predict these quantities should be utilized in the design phase.

The physical space, or "real estate," occupied by an inductor may also be an important issue for the designer. Different inductor configurations, including multilayered 3-D structures, may be evaluated depending on the particular application and design constraints. The CAD oriented models described in this chapter may be extended to such multilayered and embedded spiral inductors. Figure 2.2 shows the low frequency inductance for a single and two layer structure embedded in a layered medium such as LTCC or FR-4 [12] as a function of the number of turns. Multilayer structures can be connected in parallel to decrease the resistance and increase the inductor Q. Potential advantages of 3-D designs are lower EMI as a result of reduced aperture area, as well as lower series resistance for a given inductance value, with the former also applying to single layer spirals embedded in multilayered media.

Dielectric losses in multilayered media may also be calculated. As an example, we consider quality factor for spiral metallization on oxide layers over a typical silicon substrate ($\sigma = 1$ S/m). The quality factor based on dielectric losses exclusively, Q_{dl}, can be computed as

$$Q_{dl} = \frac{\omega\sqrt{\mu_o \epsilon_o \epsilon_{eff}}}{\alpha} \tag{2.1}$$

where α is the attenuation constant and ϵ_{eff} is the effective dielectric constant associated with the transmission line representing the metal trace on the oxide layer. Upon observation of the plot of Q_{dl} versus frequency in Figure 2.3, it is clear that

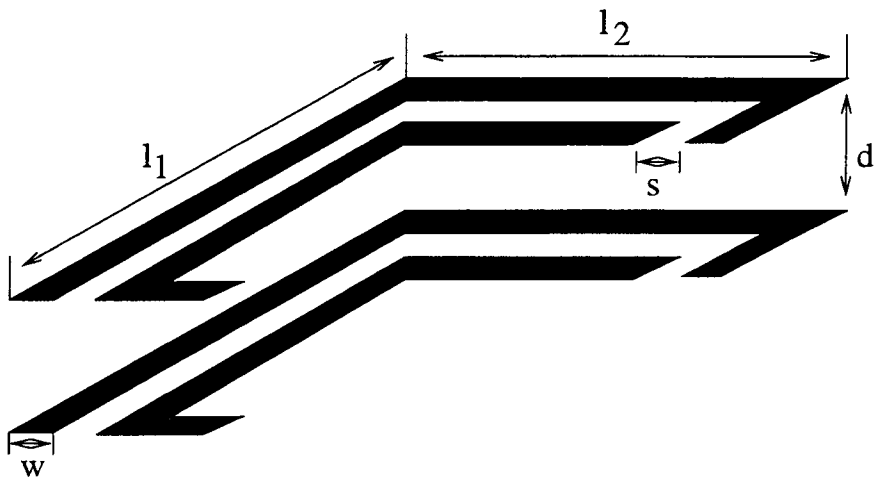

(a)

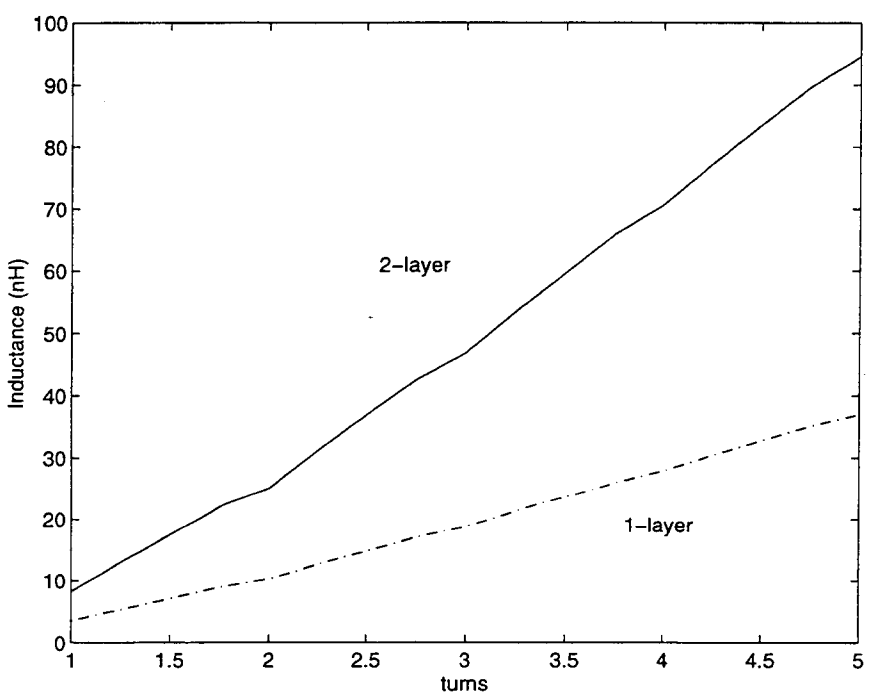

(b)

FIGURE 2.2. Inductance vs. number of turns for single and two layer spirals, $l_1 = l_2 = 0.1$cm, $w = s = 0.002$cm, $t = 0.00025$cm, and separation distance $d = 0.01$cm for the two layer structure

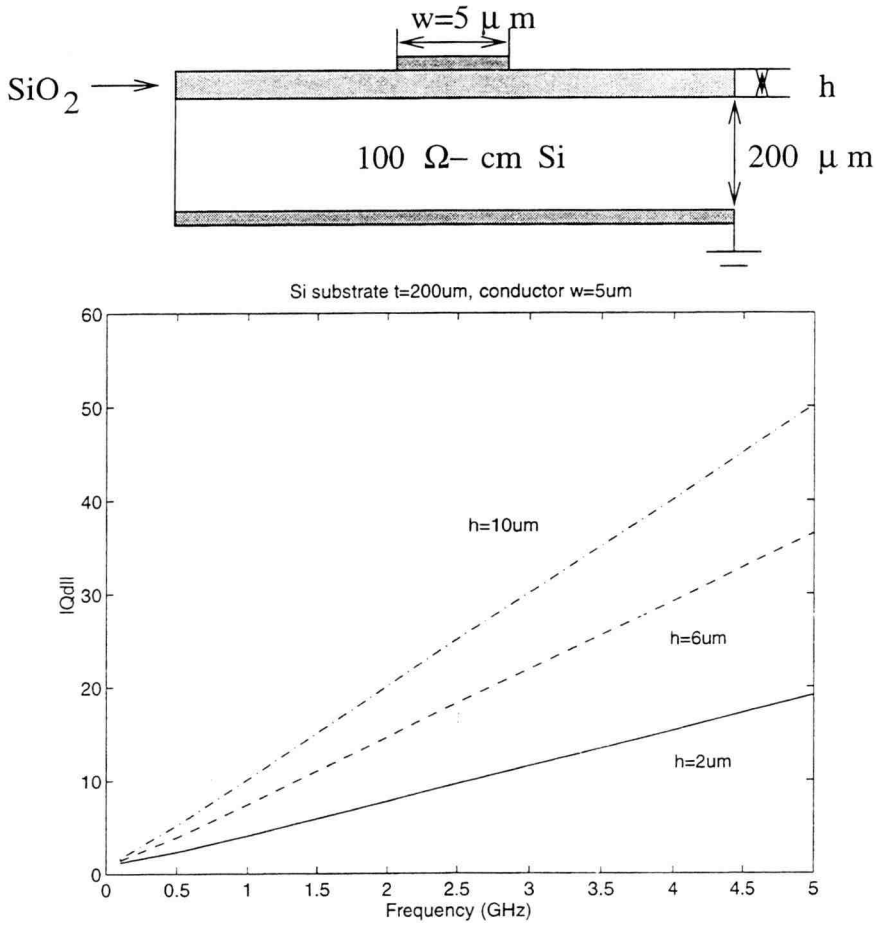

FIGURE 2.3. Quality factor, Q_{dl}, vs. frequency for conductors h=2, 6, and 10 μm above a 200 μm Si substrate.

for inductors implemented in such Si-based ICs, the structures should be fabricated on the thicker oxide layers or second or third level metallization layers in order to maximize quality factor.

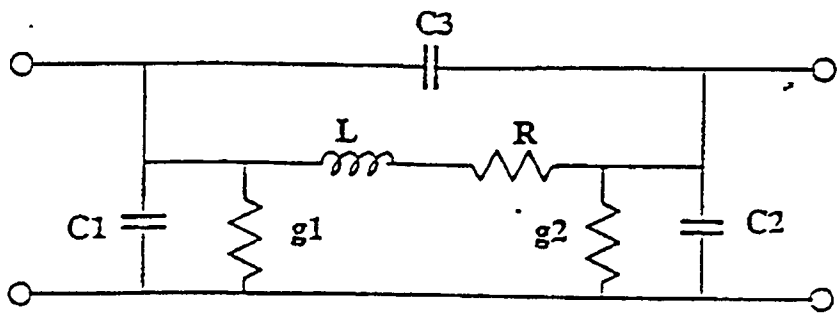

FIGURE 2.4. Equivalent circuit model for spiral inductors

2.4. Modeling Techniques

A CAD oriented equivalent circuit model, shown in Figure 2.4, has been developed for the spiral inductors [1], which may be extended to multilayered structures. The method for constructing the equivalent circuit for a rectangular spiral employs a modified Geometric Mean Distance (GMD) [3] formulation, incorporating dielectric and radiation losses and ground plane effects. For a straight planar conductor segment, the self inductance, L_o, is calculated as,

$$L_o = 2l[\ln(2l/(w+t)) + 0.50049 + (w+t)/(3l)] \quad (nH) \tag{2.2}$$

where w and t are the width and thickness in centimeters. For two parallel lines of equal length, l, and GMD separation in centimeters, the mutual inductance is found by the following expression,

$$M_{ij} = 2lQ \quad (nH) \tag{2.3}$$

where

$$Q = \ln\left[(l/GMD) + [1 + (l^2/GMD^2)]^{1/2}\right] - [1 + (GMD^2/l^2)]^{1/2} + (GMD/l) \quad (2.4)$$

Inclusion of the ground plane effect is accomplished by solving the mutual inductance problem with an image inductor of opposite current polarity at a separation distance twice that of the substrate height. An appropriate combination of these terms leads to the total inductance including a ground plane, and is of the form

$$L_T = \sum_i L_o^i + \sum M_{ij} + \sum M_{ij}^g \quad (2.5)$$

Capacitance values for a structure must also be calculated to yield an accurate frequency dependent inductance estimate. Both even and odd mode capacitances may be calculated via the closed form expressions given in [1], as well as fringing capacitances. These can then be easily incorporated into the equivalent circuit model.

Ohmic losses are calculated using the skin effect frequency dependent resistance formulae given in [13]. The series resistance, R, of the equivalent circuit also includes a radiation loss term given by

$$R_r = \frac{2}{\eta}\left|\frac{\omega\mu_o}{\lambda}\right|^2 \cdot \sum_{n=1}^{N} S_n \left[\frac{1}{3} + \frac{cos(2kh)}{(2kh)^2} - \frac{sin(2kh)}{(2kh)^3}\right] \quad (2.6)$$

where η is the wave impedance, S_n is the average cross sectional area for each of the N turns, and k is the wavenumber. Equation 2.6 is derived by approximating each turn of the spiral as a magnetic dipole and then summing the contributions of each turn to the radiation resistance to arrive at the final expression above.

In addition, the radiation pattern associated with a typical spiral may be calculated from the following expressions for radiated electric and magnetic fields, for inductors with and without a ground plane, respectively,

$$H_\theta = -\frac{k^2 I_o \sum_{n=1}^{N} S_n sin(\theta)}{2\pi r} sin(khcos(\theta))e^{-jkr}$$
$$E_\phi = \frac{\eta k^2 I_o \sum_{n=1}^{N} S_n sin(\theta)}{2\pi r} sin(khcos(\theta))e^{-jkr} \quad (2.7)$$

and

$$H_\theta = -\frac{k^2 I_o \sum_{n=1}^{N} S_n sin(\theta)}{4\pi r} e^{-jkr}$$
$$E_\phi = \frac{\eta k^2 I_o \sum_{n=1}^{N} S_n sin(\theta)}{4\pi r} e^{-jkr} \tag{2.8}$$

where I_o is the current. The EMI in high density modules caused by radiation from embedded inductors can be of critical importance for a reliable design. An estimate of the coupling effects due to radiation from these RF components may then be obtained using the above expressions. As an example, consider the mutual impedance between two coplanar loops above a ground plane, which can be calculated as,

$$Z_{12}^m = \frac{j\omega\mu_o \sum_{n1=1}^{N_1} S_{n1}^1 \sum_{n2=1}^{N_2} S_{n2}^2 k^2}{4\pi} \cdot \left[\frac{2hd}{(d^2+4h^2)^{3/2}} e^{-jk\sqrt{d^2+4h^2}} - \frac{e^{-jkd}}{d} \right] \tag{2.9}$$

Here h and d represent the substrate height and separation distance respectively. Figure 2.5 shows the radiation pattern of an isolated spiral and the mutual inductive coupling at 1 GHz with an identical coplanar spiral as a function of distance. The mutual inductive coupling may also be evaluated using simple GMD-based formulations or other advanced techniques, such as those based on rigorous analysis of near zone fields.

2.5. Simulations and Measurements

For model verification, an experimental 10X structure was fabricated and tested on a Vector Network Analyzer (VNA), using single port reflection (S_{11}) data. The modified GMD-based method is used here to calculate the equivalent circuit model for the single layer three turn rectangular spiral shown in Figure 2.6, with 1 mil copper conductor on a 10 mil duroid ($\epsilon_r = 2.2$) substrate. Figure 2.7a shows the predicted and measured inductance of the spiral as a function of frequency. Although

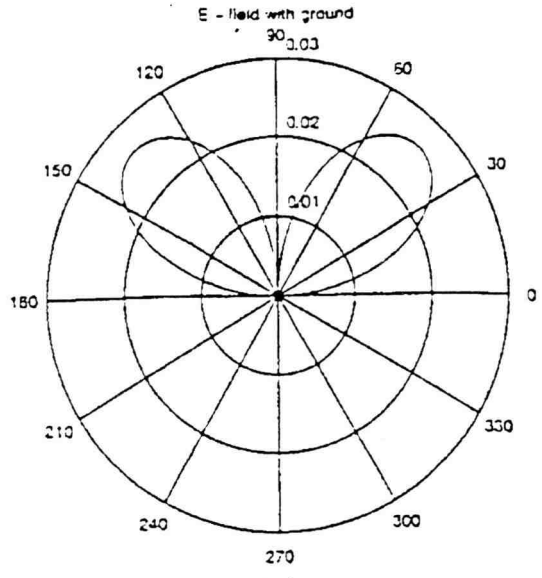

(a)

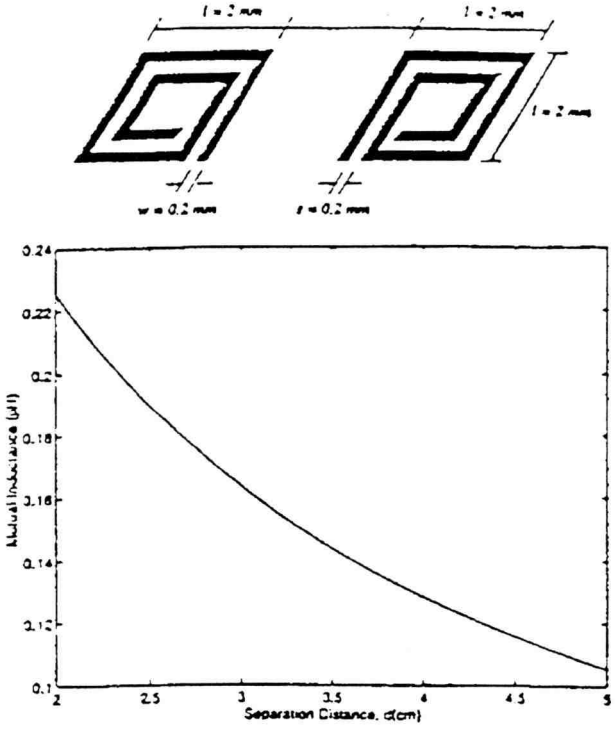

(b)

FIGURE 2.5. a) Radiation pattern of isolated spiral and b) mutual coupling between two identical coplanar spirals as a function of distance at 1 GHz

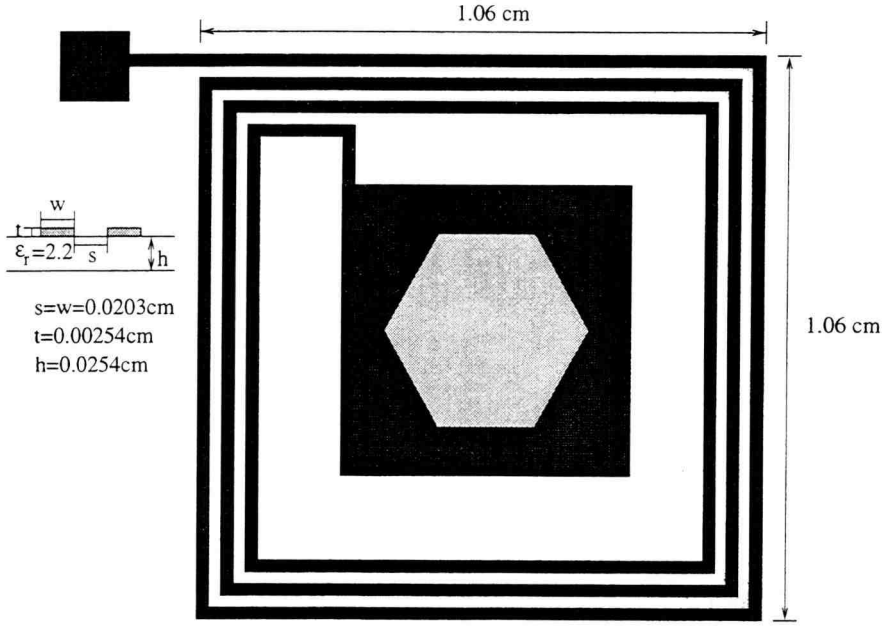

FIGURE 2.6. Schematic of the 3-turn rectangular spiral

the modified GMD model provides a conservative estimate for inductance, the usable frequency range and resonant frequency are in good agreement.

Quality factor was also calculated from the VNA reflection measurements. A comparison of measured and simulated Q factors is shown in Figure 2.7b. Q values between 20 and 25 were obtained for a frequency range of $75 - 250$MHz.

2.6. Conclusion

In conclusion, CAD oriented modeling techniques may be used to simulate the performance of spiral inductors in multilayered media. The design methodology presented has been validated by experimental VNA measurement. Inductor parameters such as usable frequency range, near and far field coupling estimates, and quality factor are extractable from the models which can be used in the design phase of RF or mixed signal modules.

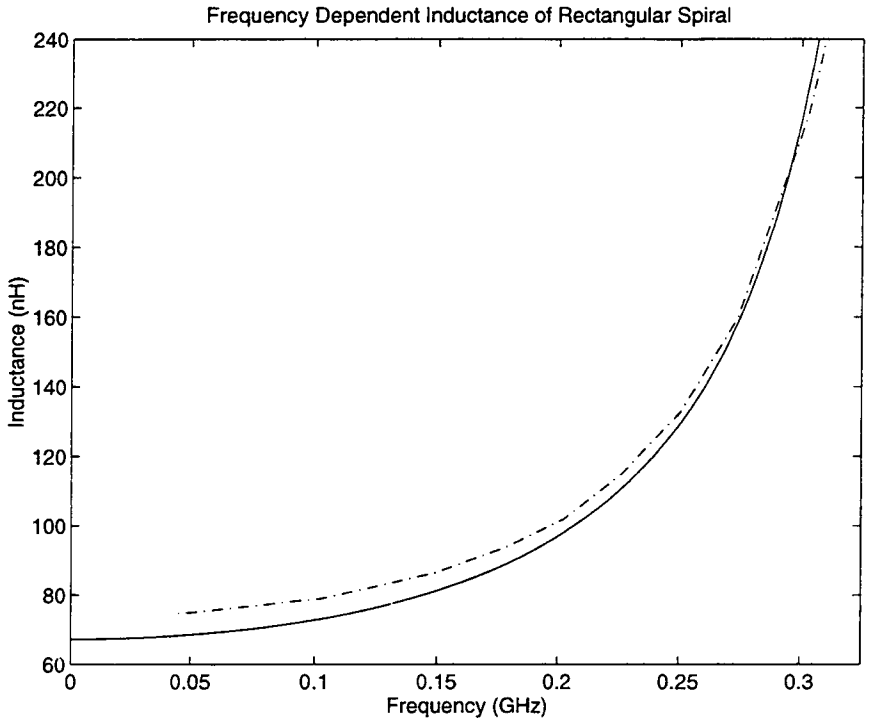

(a)

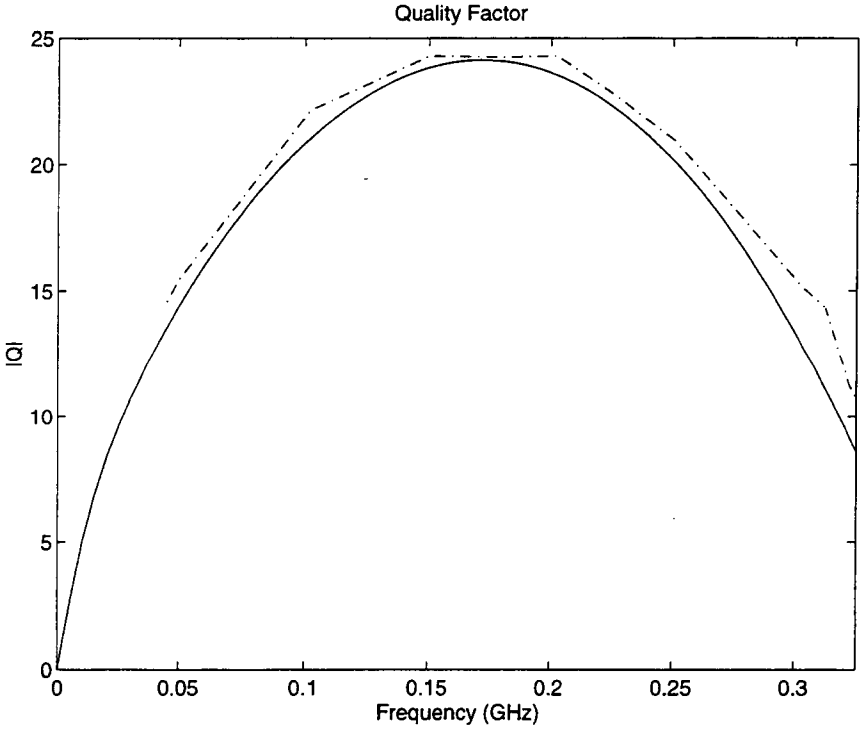

(b)

FIGURE 2.7. a) Inductance and b) Quality Factor as functions of frequency, – simulated, -· VNA measurement

3. ANALYSIS AND MODELING OF SPIRAL INDUCTORS IN LOSSY MEDIA

3.1. Introduction

As standard silicon-based circuit technologies are being used for higher frequency designs, their usage for implementing microwave structures has also become a topic of recent interest. A primary component of many monolithic microwave integrated circuit (MMIC) and RFIC designs is a spiral structure used to realize an inductive element. One major concern facing designers contemplating the fabrication of such spirals in a silicon-based environment is the resulting poor quality factor due to lossy substrates and high resistivity metallization when compared to inductors manufactured in other established microwave media, such as GaAs [1]. However, lower fabrication costs make these structures attractive, as long as reasonable performance can be achieved.

3.2. Microstrip in Si-SiO_2

Microstrip structures fabricated in lossy substrate processes, such as those in CMOS and bipolar technologies, are a topic of continued interest due to the need to implement transmission line structures for on-chip interconnects as well as producing other traditional microstrip structures on-die, such as filters, MIM capacitors, and spiral inductors. While the properties of microstrip lines above lossy media have been studied extensively in [4] and [5], current modeling techniques for spirals above lossy substrates have not properly incorporated all substrate effects, particularly substrate currents, which can have a dominating effect for certain frequencies, substrate conductivities, and geometries. Hence, a general analysis of the

substrate effects and development of a modeling technique are necessary for both simple single-level spirals (SLS) as well as more complex structures such as the designs described in [14]- [16].

First, we consider propagation characteristics of an Si-SiO_2 microstrip configuration as a basic element of the planar spiral inductor. The planar conductor is above a double layer substrate consisting of oxide over bulk silicon. As described in the literature [4], three fundamental modes, namely, slow-wave, skin-effect, and quasi-TEM, will propagate in such a system, each having a certain frequency range for a given set of material parameters. Of particular interest for the case of the microstrip spirals in CMOS technology is the skin-effect mode, as this is the propagating mode near the first resonance.

The skin-effect mode begins to propagate when the skin depth δ is on the same order as or less than the silicon substrate height. In other words, with increasing frequency, the semiconducting substrate begins to behave as a lossy conductor wall and the longitudinal currents, which lower inductance per unit length, are closer to the silicon/cilicon oxide (Si/SiO_2) interface. One method of analyzing the series impedance terms of this structure is through application of Wheeler's method (incremental inductance rule) [17], which yields an inductance and associated loss that are both frequency dependent. An equivalent circuit model for a Si-SiO_2 coupled microstrip line configuration is shown in Fig. 3.1. The capacitances and shunt conductances are determined via a quasi-static Spectral Domain Analysis (SDA) [18] with complex dielectric constants. The equivalent shunt elements may be determined by evaluating the structure using SDA at one frequency and then forming the model topology, which in turn yields an overall frequency dependent capacitance and conductance that are in agreement with SDA results over a broad range of frequencies. The relationship between C_{sub} and G_{sub} is taken as,

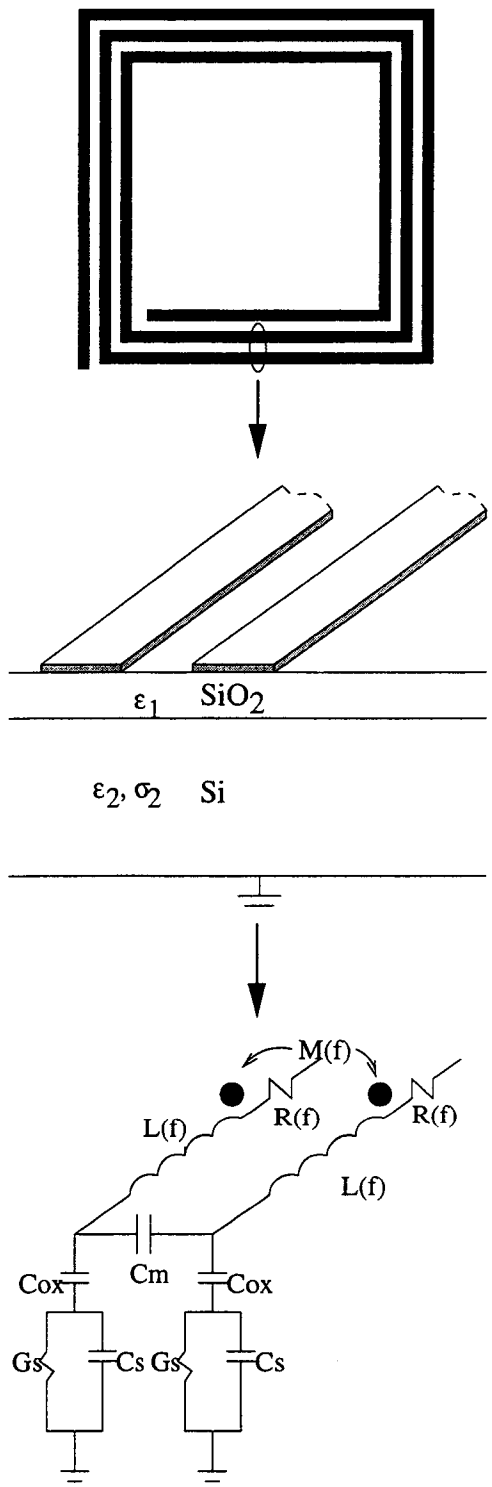

FIGURE 3.1. Equivalent circuit for Si-SiO_2 microstrip coupled lines in skin effect mode

$$G_{sub} = \frac{\sigma_{sub}}{\epsilon_{sub}} \cdot C_{sub}, \tag{3.1}$$

which is based entirely on the physical nature of the structure and also provides a unique solution for the conductance and both capacitance values. Distributed inductances and resistances are calculated using a modified Partial Element Equivalent Circuit (PEEC) [19] methodology including a frequency dependence to account for the skin effect mode. The frequency dependent series resistances incorporate the effects of finite skin depth in the metallization as well as loss in the semiconducting substrate. The substrate losses due to longitudinal currents are computed by finding the quasi-static solution to the magnetic vector potential equation in each layer i [6]

$$\nabla^2 A_{zi}(x,y) = j\omega\mu_o\sigma_i A_{zi}(x,y) \tag{3.2}$$

where z is the direction of propagation, subject to the appropriate boundary conditions (e.g. $A_z = 0$ on the ground plane). In the semiconducting substrate region, the current density is computed as

$$J_z(x,y) = -j\omega\sigma_{sub} A_z(x,y) \tag{3.3}$$

Fig. 3.3 shows the current density below the oxide as a function of frequency and depth for a typical Si-SiO_2 microstrip structure with $h_{ox} = 4\mu$m, $h_{sub} = 120\mu$m, and $\sigma_{sub} = 10^4$ S/m. Similarly, Fig. 3.2 displays the normalized longitudinal current density, $\bar{J}_z$, in a cross section of the substrate directly below a unitary filament of current for various frequencies. It can be deduced that there is current crowding in the vertical direction at the substrate/oxide interface, and also in the horizontal direction in the area beneath the strip, as evidenced by the overall magnitude increase of the peak longitudinal substrate current density with frequency.

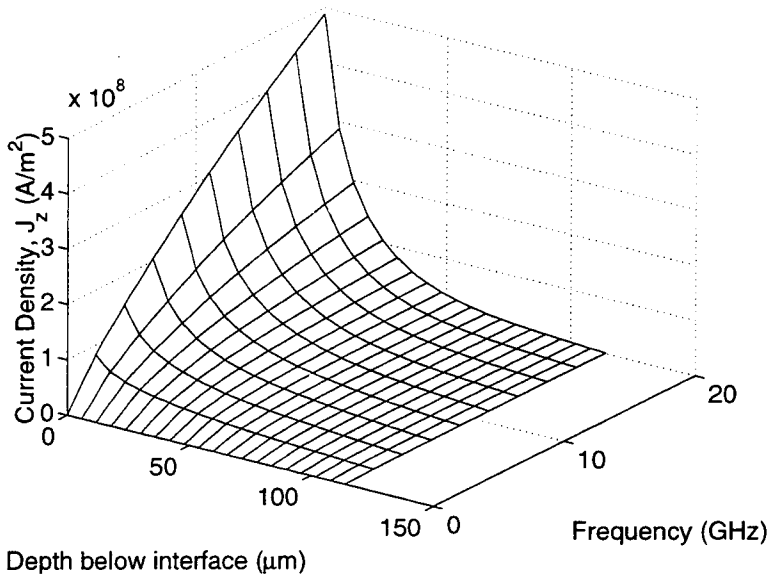

FIGURE 3.2. Longitudinal substrate current density vs. frequency and depth below oxide/Si interface

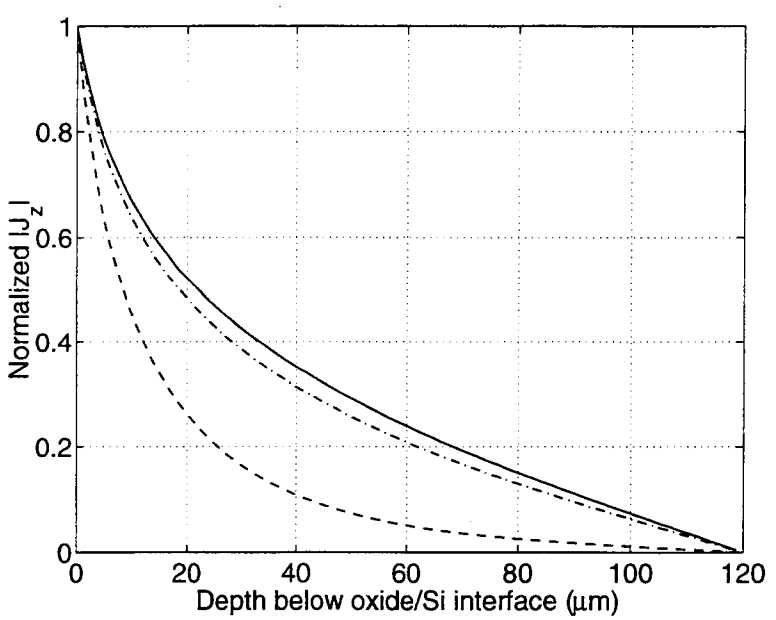

FIGURE 3.3. Normalized longitudinal substrate current density for f= 0.001 GHz (–), 0.1 GHz (-·) and 10 GHz (- -)

3.2.1. Line constants: r, l, g, and c

An examination of the per unit length (p.u.l.) line constants r, l, g, and c, of a single microstrip structure provides insight into the mechanisms behind the three propagation modes and the transitions between them. Here the behaviors of these line constants for a typical MIS microstrip structure are discussed.

For low values of σ_{sub}, shunt capacitance and conductance are minimized, and correspondingly inductance is maximized and series resistance minimized, resulting in a quasi-TEM dielectric propagation mode for the two-layer microstrip structure. The minimization of the shunt elements can be explained by viewing the double layer substrate as a series connection of two capacitances with the semiconducting capacitance being complex. Thus, when σ_{sub} is zero, the total shunt capacitance is real and minimum in magnitude, and conversely as σ_{sub} goes to ∞, only the insulating layer capacitance remains since the semiconducting substrate capacitance is maximum and almost completely imaginary (i.e. a pure shunt conductance). It is also intuitive that the series impedance value becomes completely inductive when σ_{sub} is zero (assuming zero metallization loss) since there are no losses due to longitudinal currents in the semiconducting substrate. In addition, this inductance is the maximum value for the structure, as any longitudinal substrate currents would be opposing the current in the strip and only serve to reduce the total magnetic flux linkage.

For moderate values of σ_{sub} and relatively low frequencies, a so-called slow-wave mode propagates. The reasons behind this behavior become evident when the capacitance values are examined. Considering that capacitance is a monotonically increasing function of σ_{sub} for a fixed frequency, it is clear that if inductance does not decrease significantly while capacitance increases, then the phase velocity, which

is proportional to $1/\sqrt{LC}$, will be lower. Thus, the mode of propagation in this case is a 'slow'-wave mode. Another way to view this phenomenon is from the energy storage perspective. The magnetic energy storage mechanism is essentially that of an air-filled microstrip structure, whereas electric energy is stored almost completely in the insulating substrate layer and air above the strip, as this is the dominant shunt capacitance for this mode. Thus, as pointed out in [4], the energy transfer across the interface results in a slower propagation velocity.

The skin depth, δ, of a material for a given frequency is a measure of the electromagnetic field penetration into the medium and is useful in general for structures with dimensions on the same order of or greater than δ. When we consider the case for which $h_{sub} > \delta$, there are significant implications for the series impedance terms, r and l. As σ_{sub} increases, the current density in the semiconducting substrate also rises. This reduces inductance as current of opposing polarity is flowing closer to the strip conductor, thus reducing flux linkage and consequently the net inductance. Resistance rises in accordance with the increasing current density and resultant crowding in the semiconducting substrate below the strip.

To exemplify the behaviors of the line constants and the associated modes, Figures 3.8, 3.7, 3.6, and 3.5 display r, l, g, and c as functions of frequency and lower substrate conductivity for a typical MIS structure, shown in Figure 3.4. The ranges of σ_{sub} for each plot have been chosen to show the greatest amount of change in each of the line constants for the given frequency range, the same in all four cases. The fact that the transitions for r,l,g, and c do not all occur in the same frequency range provides insight into why the three fundamental modes exist. In general, a typical MIS structure with a relatively high ($> 10^3$ S/m) lower substrate conductivity will exhibit all three modes, beginning with slow-wave, then transitioning in the skin-effect mode and finally the quasi-TEM dielectric mode.

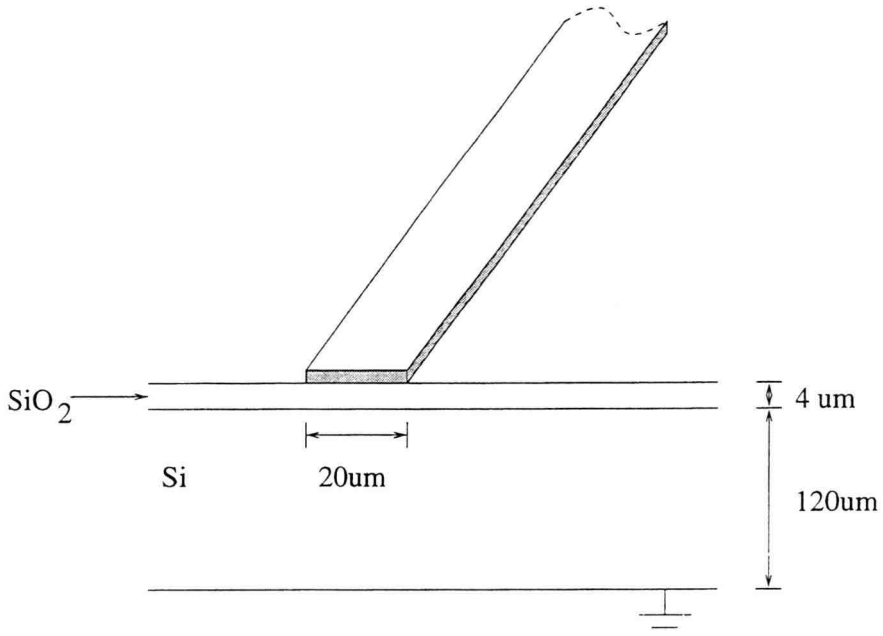

FIGURE 3.4. Example Si-SiO_2 microstrip structure

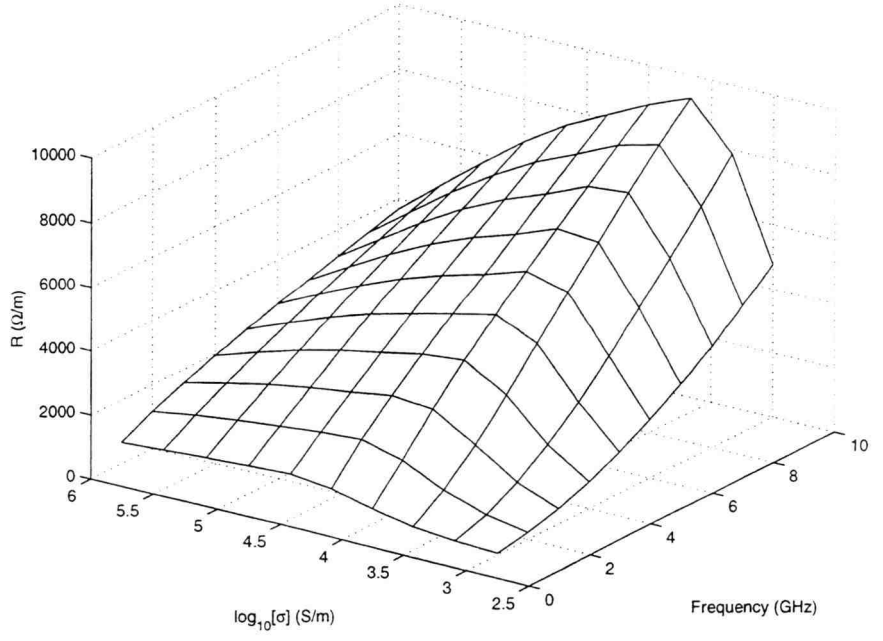

FIGURE 3.5. Resistance p.u.l. as a function of frequency and lower substrate conductivity

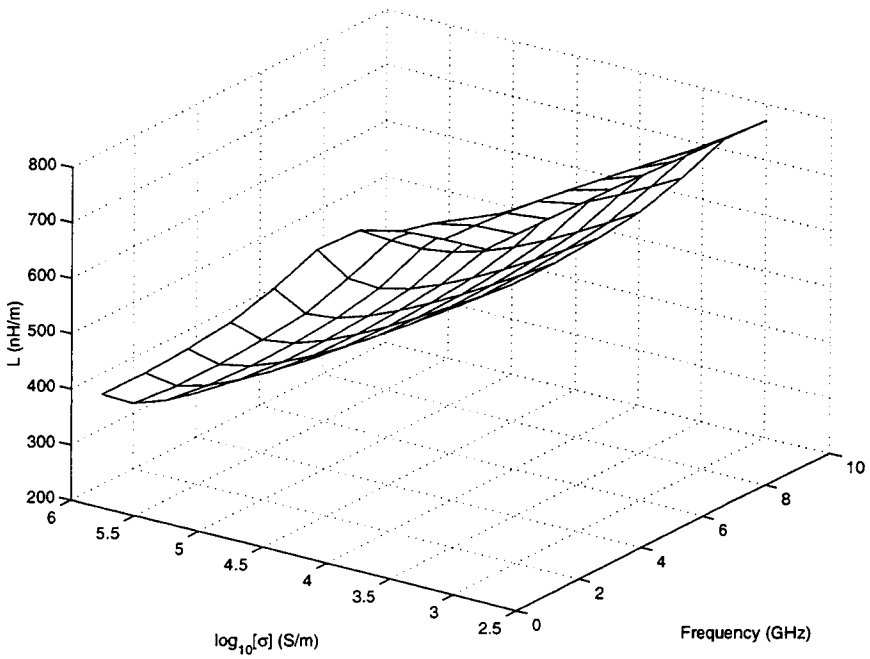

FIGURE 3.6. Inductance p.u.l. as a function of frequency and lower substrate conductivity

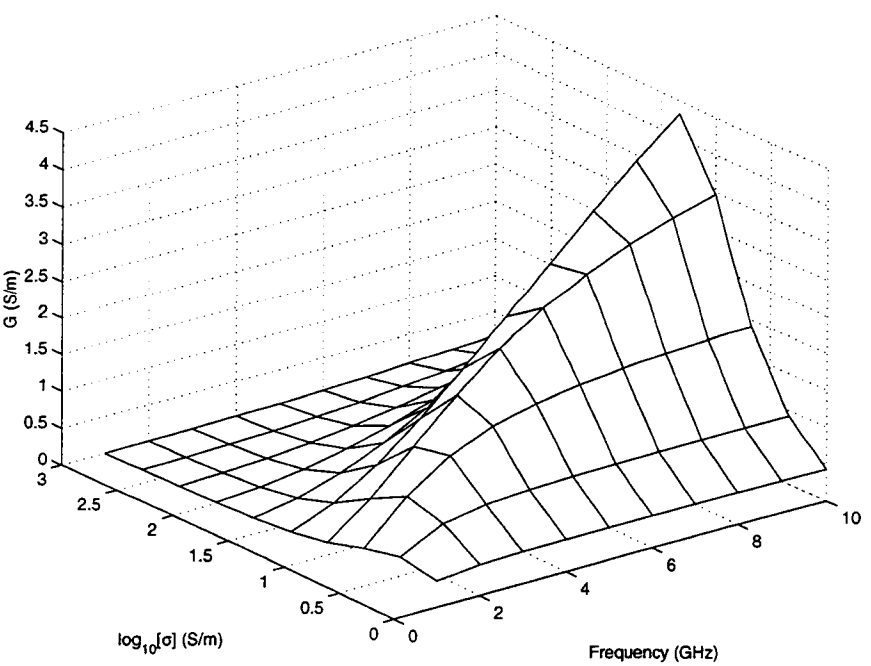

FIGURE 3.7. Conductance p.u.l. as a function of frequency and lower substrate conductivity

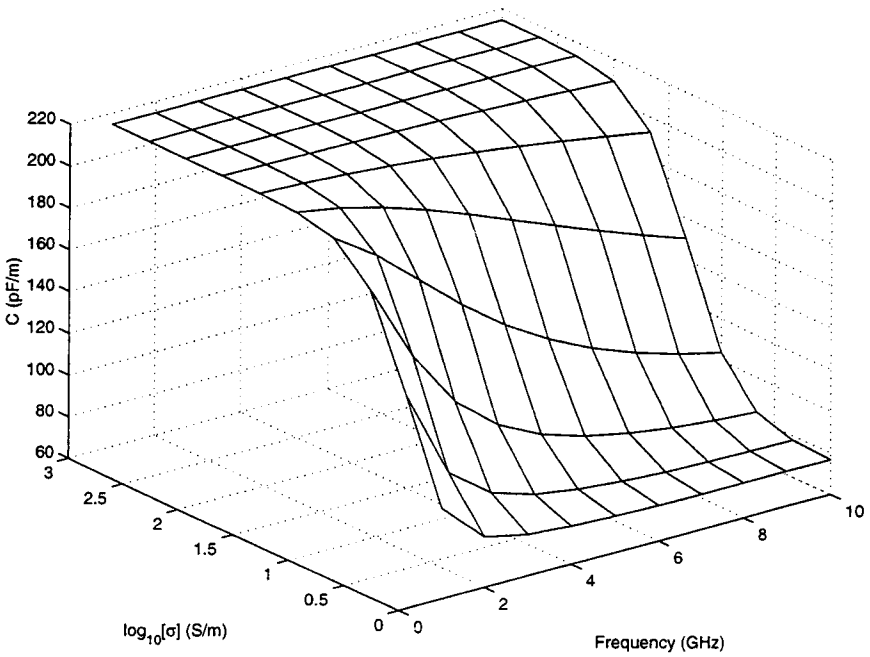

FIGURE 3.8. Capacitance p.u.l. as a function of frequency and lower substrate conductivity

3.2.2. Mutual Capacitance and Inductance

The mutual reactive immitance terms for a coupled line system are also adversely affected by the presence of a conductive substrate. Figure 3.10 shows the mutual inductance and capacitance for a two line structure shown in Figure 3.9. As for self inductance, the mutual inductance decreases with increasing frequency due to larger longitudinal substrate currents. The increase in mutual capacitance for lower substrate conductivity is due to higher displacement current through both dielectrics. This behavior may be interpreted as follows, at low frequencies a dielectric layer with a finite conductivity will have primarily conduction currents while above a particular frequency the displacement current will dominate. The frequency

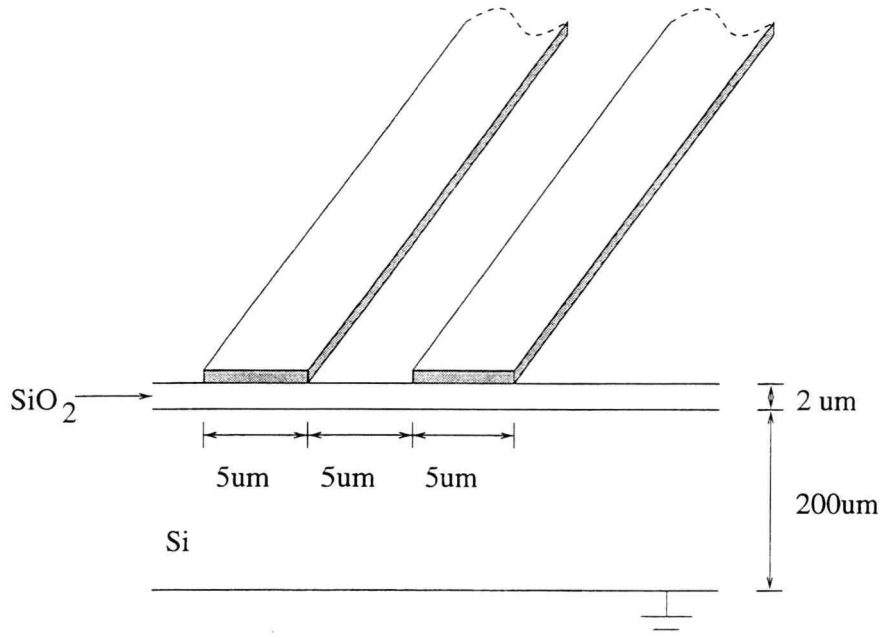

FIGURE 3.9. Example Si-SiO_2 coupled microstrip line structure

range in which this transition between conduction and displacement current occurs is directly proportional to σ_{sub}.

3.3. Overview of Modeling Techniques for Spirals in Lossy Media

A number of design techniques have been proposed and tested for spirals in lossy media, including use of multiple metallization layers connected in parallel [14] and/or high resistivity Si substrates [15], as well as air-suspended spiral designs [16]. A spiral's inductance, quality factor, and self-resonant frequency are key design considerations. Any scalable models developed must be able to accurately predict such figures of merit. In order to model the Si-based spirals, a CAD-compatible method incorporating GMD and Partial Element Equivalent Circuit (PEEC)-based inductance calculations [3, 19], and Spectral Domain Analysis (SDA)-based compu-

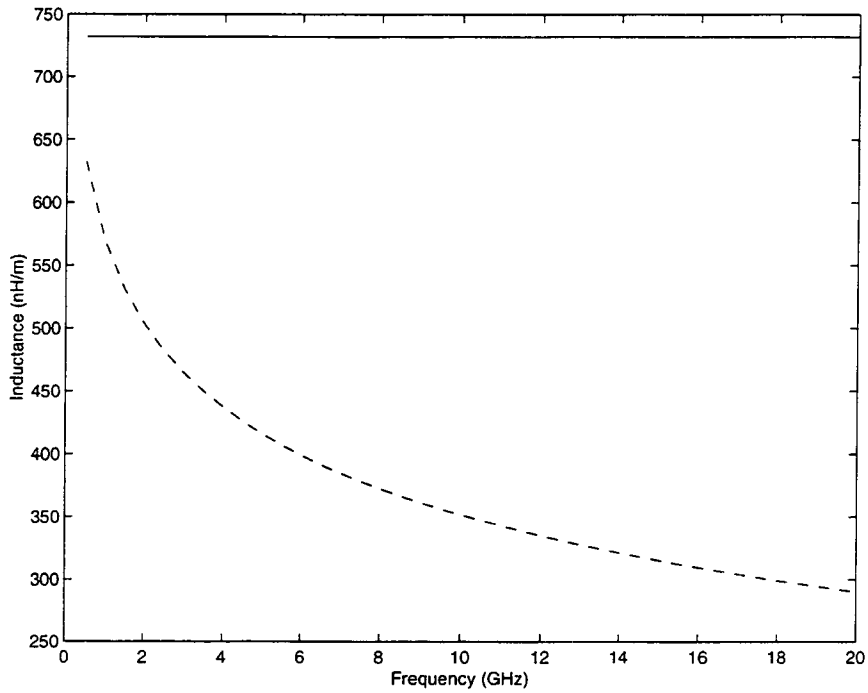

(a)

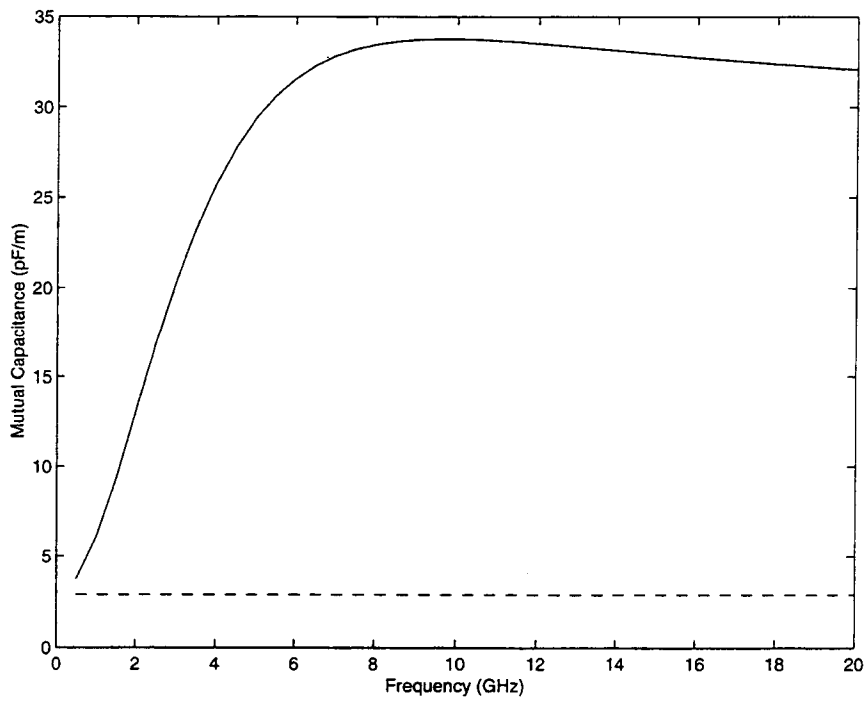

(b)

FIGURE 3.10. Comparison of mutual a) inductance and b) capacitance p.u.l. versus frequency for $\sigma_{sub} = 10$ (solid), 10^4 (dashed) S/m

tation of capacitances and conductances [18], is implemented. The resulting scalable circuit model includes the effects of frequency dependent reactances and the associated losses due to semiconducting substrates, imperfect dielectrics, and conductor metallization for spiral designs, and thus allows for optimization of performance for a desired inductance and frequency range.

3.3.1. Partial Element Equivalent Circuits (PEEC)

Partial Element Equivalent Circuit (PEEC) [19] models are derived from integral equation solutions based on the summation of all electric field sources within a conductor geometry,

$$\frac{\bar{J}}{\sigma} = \bar{E}_o - \frac{\partial \bar{A}}{\partial t} - \nabla\Phi \tag{3.4}$$

and their respective time and spatial dependence. The three main computational tasks involved are inductance calculations, capacitance calculations, and network analysis.

Formulation of a PEEC model first requires that a structure be broken down into volume cells which form a basis for the nodes in the final PEEC. The unknown quantities (i.e. current and charge) are assumed to be locally constant within their respective cell boundaries. Thus the equivalent circuit element values may be calculated and utilized in solving the integral equation for a single cell or between two cells, the latter applying to mutual inductive and capacitive terms. Inductance and capacitance values may be calculated via the closed form expressions presented in [20]- [21]. The resulting equivalent circuit model then consists of partial self and mutual inductances and capacitances, with the number of each being determined by the number of nodes and significant coupling terms (L_{pij}, C_{pij}) included.

Time retardation effects may also be included in the PEEC models for geometries having dimensions which are large in comparison to wavelength. For a region with uniform properties ϵ_r, μ_r, the retarded time is given by,

$$t' = t - \frac{|\bar{r} - \bar{r}'|}{c}(\epsilon_r \mu_r)^{1/2} \tag{3.5}$$

where $\bar{r}$ and $\bar{r}'$ are vectors from the origin and c is the speed of light. While a retarded PEEC model solver is more difficult to implement due to the delays, the difference between the retarded and non-retarded solutions may be significant enough to warrant the extra analysis efforts [22]. For EMI problems, the far coupling terms can have appreciable phase lags associated with them when the spectrum of the excitation contains frequencies such that the condition $\tau_{ij} f_{max} << 1$ is no longer satisfied.

PEEC models which do not include retardation are entirely CAD compatible, as they consist solely of lumped elements with mutual coupling. Thus, any popular simulation tool, such as Libra and MWSpice©, may be used to obtain frequency or time domain descriptions for any node in the network.

The PEEC methodology lends itself well to the analysis of multiconductor systems with three dimensional geometries. Such a class of conductor arrangements includes multilayered lumped elements. Although the standard PEEC methodology can be used to compute both the inductances and capacitances associated with the spirals, an alternate efficient and accurate spectral domain technique for the computation of capacitances and conductances associated with structures on semi-insulating silicon substrates [18, 23, 24] is used for the models contained herein. Spiral inductors which have their 'windings' on multiple metallization levels can be accurately modeled by a PEEC description which incorporates coupling between

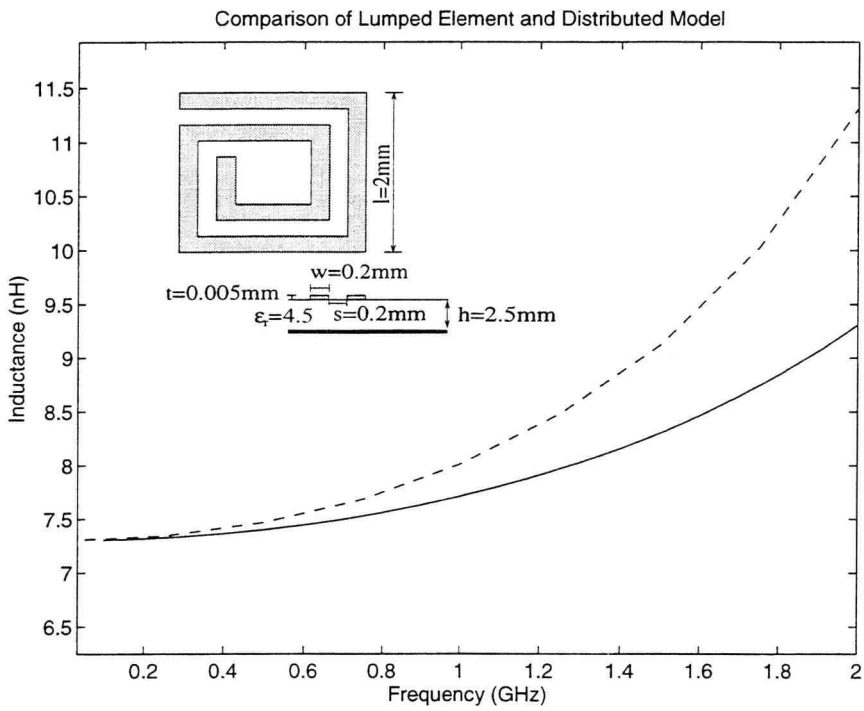

FIGURE 3.11. frequency dependent inductance for 2-turn spiral using simple lumped element (dashed) and distributed PEEC-based (solid) models

the different levels. This significantly reduces the analysis efforts over conventional three dimensional modeling techniques.

A model utilizing the PEEC methodology has been developed for rectangular microstrip spiral inductors. An algorithm which systematically subdivides the given geometry into appropriately sized cells forms the basis for the elements of the PEEC. Finally, ordinary matrix-based network analysis techniques are then used to obtain the nodal solution as a function of frequency for the spiral model. Typical results comparing a simple lumped circuit model and a PEEC-based model for a spiral are shown in Figure 3.11. Clearly, significant differences between the models exist at frequencies below self-resonance.

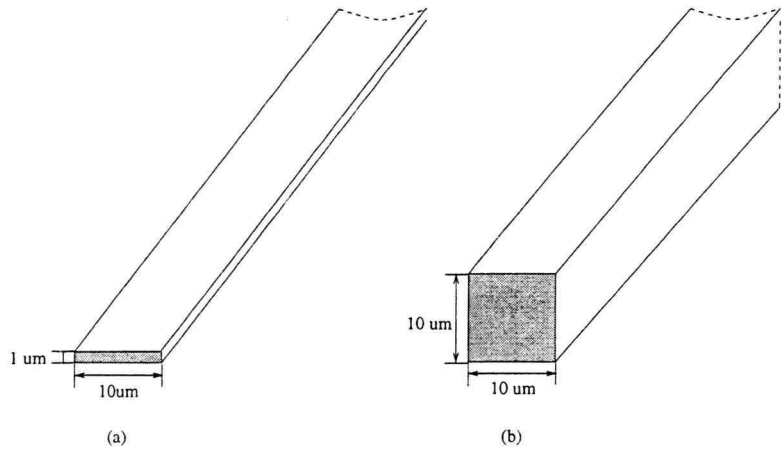

FIGURE 3.12. Structures for Figs. 3.13 and 3.14

3.3.2. Comparison of PEEC (NBS) and Greenhouse's Inductances

In order to determine the valid ranges for using the Greenhouse [3] method for calculating self and mutual inductances, the two expressions are compared with the corresponding expressions given by Hoer and Love (National Bureau of Standards) [20]. The latter equations involve full 3-D integrations over the conductors involved, thus providing a high accuracy standard for comparison. Figure 3.13 shows the inductance p.u.l. of a thin conductor (Fig. 3.12a) as a function of length using the two different methods of calculation. Greenhouse's formulation diverges from the NBS-based values for length-to-width ratios less than two. This demonstrates that for thin conductors, Greenhouse's simple formulation is sufficient for self inductance calculations for virtually all typical conductor lengths, as most inductors involve segments with lengths which are at least twice the line width.

Next, a conductor of square cross-section (Fig. 3.12b) is examined using the same metric for comparison. Figure 3.14 shows the results of these calculations, from which it can be deduced that the usable range for Greenhouse's formulation

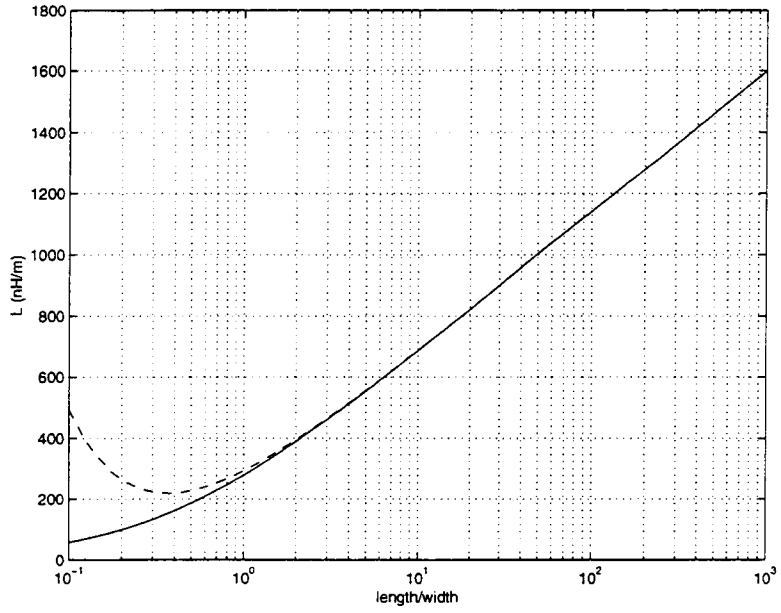

FIGURE 3.13. Inductance p.u.l. versus l/w ratio for a conductor with cross-section $1 \times 10\mu m^2$ using Greenhouse (dashed) and NBS-based (solid) methods

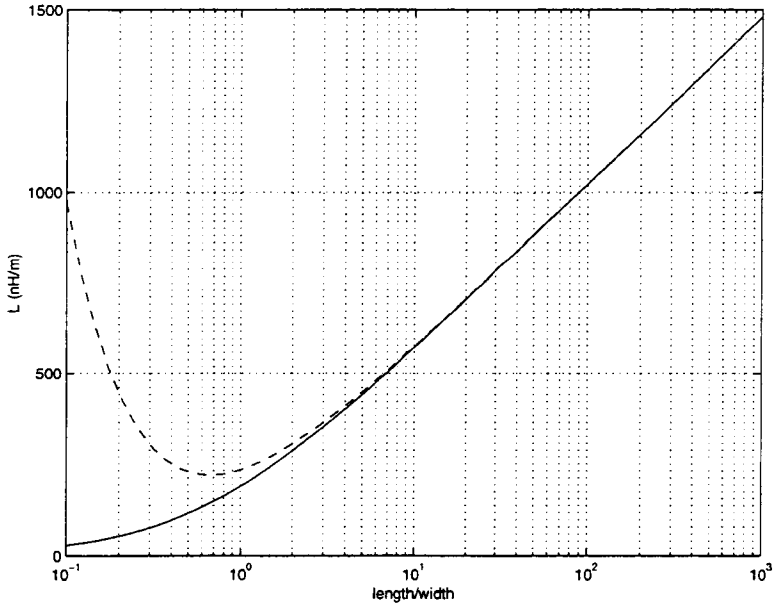

FIGURE 3.14. Inductance p.u.l. versus l/w ratio for a conductor with cross-section $10 \times 10\mu m^2$ using Greenhouse (dashed) and NBS-based (solid) methods

is reduced to lengths above approximately four times the line width. Spirals with large numbers of turns and minimized area will usually have a few short sections in the center region which are below this range, so the NBS expressions should be used in these cases.

3.3.3. Substrate Loss in Spiral Inductors

The modeling and design techniques developed for planar rectangular and circular spiral inductors in Semi-Insulating GaAs based MMICs [25]- [26] and other lossless or low loss ceramic substrates need to be modified to include both the conductor loss and substrate loss in semiconducting silicon substrate based ICs with aluminum metallization. These techniques include lumped element, distributed circuit as well as electromagnetic models which have been used to analyze and design low loss structures [1]- [8], [3]- [12], [27, 28].

As stated previously, spirals fabricated on semiconducting substrates such as in Si-based technologies have typically been plagued with losses due to the high resistivity metallization and semiconducting substrates. From the plot of Q_{dl} versus frequency in Figure 2.3, it is clear that for inductors implemented in such Si-based ICs, the structures should be fabricated on the thicker oxide layers or second or third level metallization layers in order to maximize quality factor.

Some attempts have been made to model lossy spirals on semiconducting Si substrates based on measurements for specific spirals [25] and the geometric mean distance (GMD) based expressions for inductance and approximate expressions for capacitances and conductances associated with the spiral equivalent circuit [2]. Attempts have also been made to use planar electromagnetic simulators for spiral in-

ductor models while augmenting the model to include spiral metallization resistance [29].

3.4. Spiral Model for High Substrate Conductivity

The coupled line model described in this chapter forms the basis for an equivalent circuit model for a complete spiral. Such a distributed model is constructed by subdividing the structure and computing an equivalent circuit for each straight section (or leg), l_m, including the capacitive and inductive coupling terms. However, due to the inductive coupling between sections of unequal length, the p.u.l. calculation of inductance is not suitable. Instead, the frequency dependent inductances are calculated via introduction of a virtual ground plane placed at a distance $\delta/2$ below the oxide/Si interface in accordance with Wheeler's method, as illustrated in Figure 3.15. This distributed model may become unnecessarily complex for a large number of discretizations; hence, it is desirable to have a means for model reduction. This may be accomplished via construction of an n-section ladder network, as shown in Figure 3.16, where n is the number of turns. The elements of the ladder network are given by

$$Cox'_k = \left[\sum_{m=(4k-3)}^{4k} l_m \right] \cdot Cox_{\text{p.u.l.}} \tag{3.6}$$

$$Cm'_k = \left[\sum_{m=(4k-3)}^{4k} \frac{(l_m + l_{m+4})}{2} \right] \cdot Cm_{\text{p.u.l.}} \tag{3.7}$$

$$Cs'_k = \left[\sum_{m=(4k-3)}^{4k} l_m \right] \cdot Cs_{\text{p.u.l.}} \tag{3.8}$$

$$Gs'_k = \left[\sum_{m=(4k-3)}^{4k} l_m \right] \cdot Gs_{\text{p.u.l.}} \tag{3.9}$$

$$L'_k(f) = \left[\sum_{i=1}^{4n} \sum_{j=1}^{4n} M_{ij}(f) \right] \cdot \frac{\sum_{m=(4k-3)}^{4k} l_m}{\sum_{m=1}^{4n} l_m} \tag{3.10}$$

$$R'_k(f) = \left[\sum_{m=(4k-3)}^{4k} l_m \right] \cdot R(f)_{\text{p.u.l.}} \tag{3.11}$$

The reduced model gives virtually the same performance in the frequency range of interest, which is usually from dc to the first resonance. The order of this particular circuit is, in general, high enough to approximate the response of the original distributed model with sufficient accuracy.

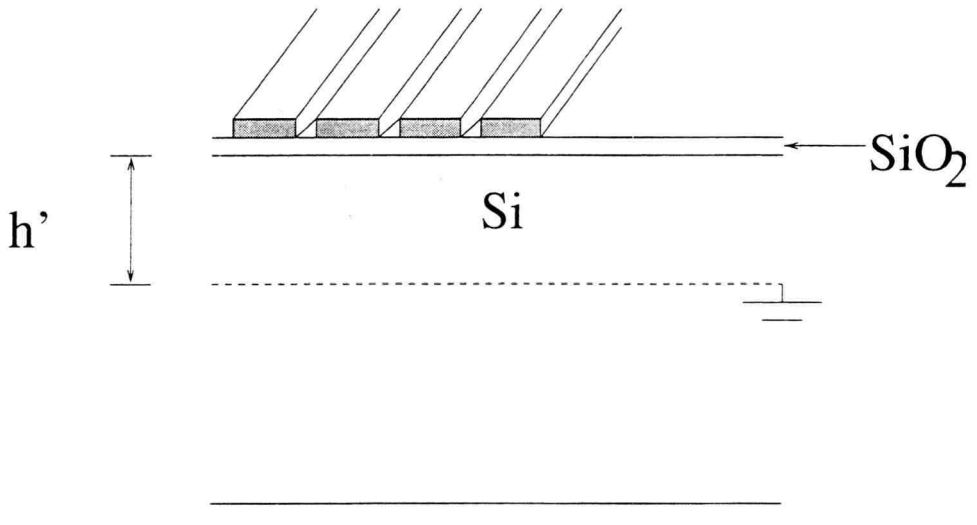

FIGURE 3.15. Use of virtual ground plane for frequency dependent inductance calculation

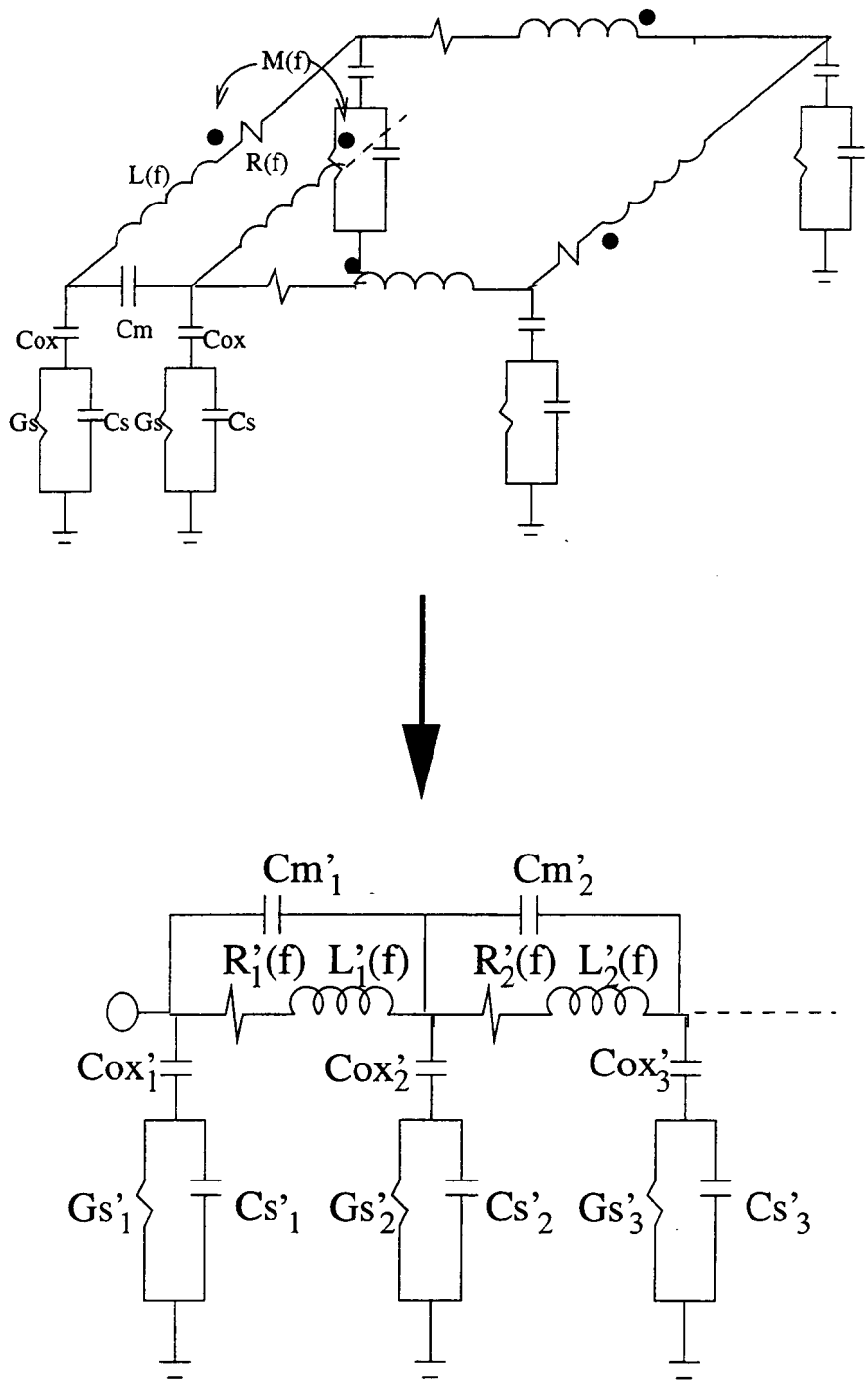

FIGURE 3.16. Synthesis of a ladder network from the distributed model for turns of a spiral inductor

4. DESIGN CONSIDERATIONS AND MODEL VALIDATION

4.1. Design Considerations

Quality factor, Q, and self resonant frequency, f_{sr}, are two key considerations when designing a spiral inductor. In the case of semiconducting media, such as in Silicon-based technologies, these two parameters may be adversely affected by the presence of a substrate with finite conductivity. Thus, any spiral design should seek to minimize these effects, with the goal of maximizing Q and f_{sr}. Design properties such as metallization resistance, substrate conductivity, geometrical dimensions, etc. are all variables which may be optimized, subject to constraints.

4.1.1. Metallization Layers

Multiple metallization layers are common in Si-based processes, which provides an additional degree of design freedom. In general, it is desirable to fabricate a spiral structure as far away as possible from a semiconducting substrate to maximize performance. To exemplify this assertion, an example single level spiral (SLS) structure is considered with oxide layer height as the variable. Fig. 4.1 shows the simulated f_{sr} and the maximum Q of a 4.5 turn spiral of area $245 \times 245 \mu\text{m}^2$ and strip width and spacing, $w = 10\mu\text{m}$, $s = 5\mu\text{m}$, on an oxide layer of varying height over the same bulk Silicon substrate ($h_{sub} = 120\mu\text{m}$, $\sigma_{sub} = 10^4$ S/m). The improvement achieved by fabricating the spiral on higher metallization layers is evident in both Q and f_{sr}. The improved Q is a result of lower substrate coupling and consequently reduced loss, while f_{sr} is observed to increase due to a lower oxide capacitance.

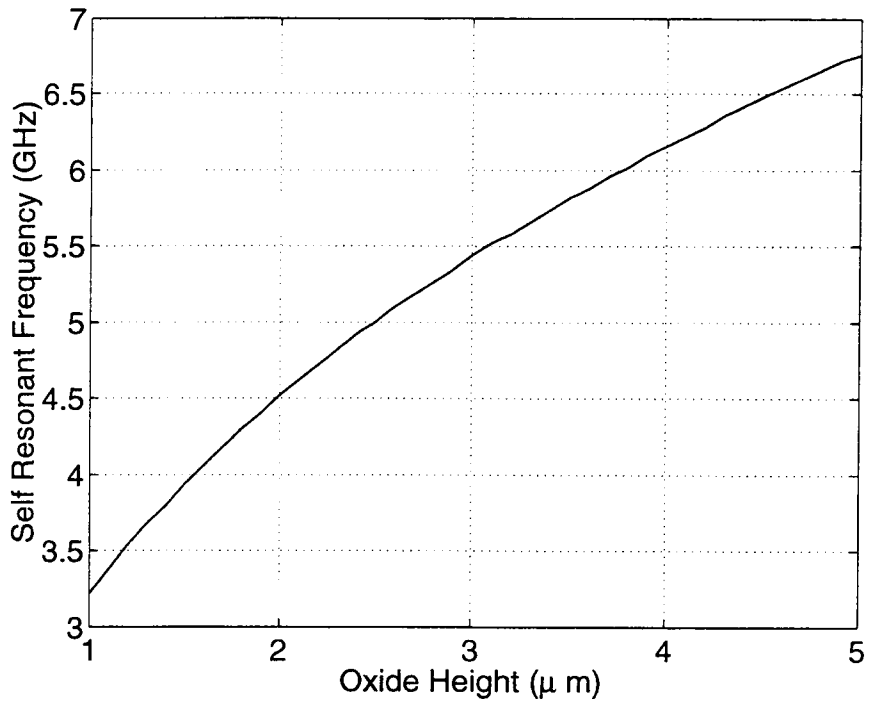

(a)

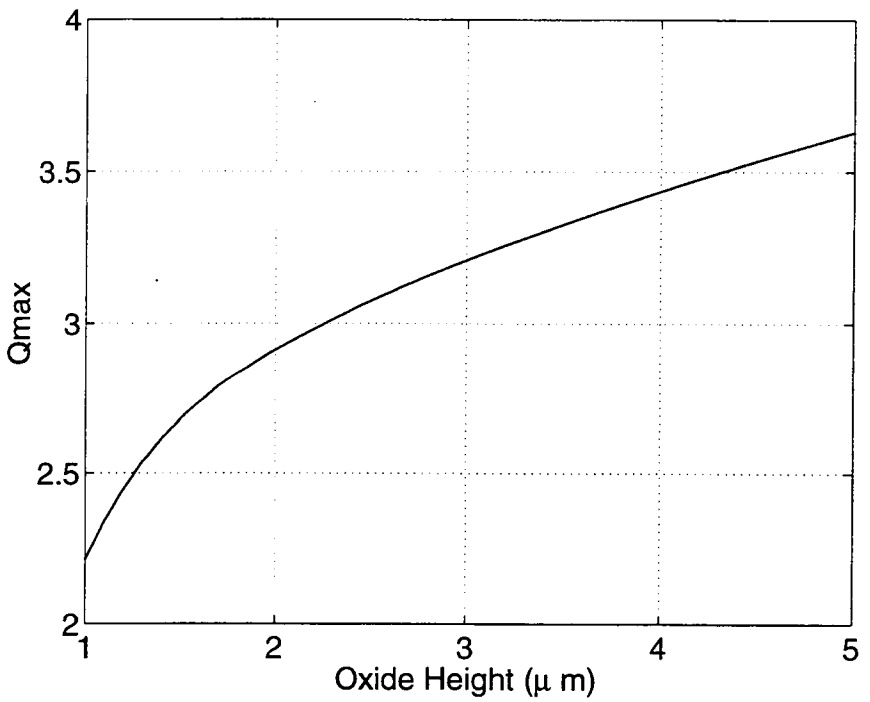

(b)

FIGURE 4.1. (a) f_{sr} and (b) Q_{max} vs. h_{ox} for a 4.5 turn SLS ($h_{sub} = 120\mu$m, $\sigma_{sub} = 10^4$ S/m)

4.1.2. Substrate Conductivity

While substrate conductivity, σ_{sub}, may not always be a variable for a fabrication process, an evaluation of its effects on performance is still in order, for it will be shown to provide insights into the valid ranges of σ_{sub} for a given application and associated design constraints.

Fig. 4.2 shows the simulated self-resonant frequency and peak Q of the same 4.5 turn spiral structure as functions of substrate conductivity. The behaviors of these two figures of merit, f_{sr} and Q_{max}, are attributable to changes in both the shunt admittances and series impedances of the microstrip sections, as well as the corresponding changes in the coupling immitance terms.

The shunt capacitance and conductance values each vary monotonically between two extrema with increasing frequency, and the frequency range in which the transitions occur are directly related to σ_{sub}. Capacitance p.u.l. varies from C_{ox} to C_{ox+s} $(= 1/(C_{ox}^{-1} + C_s^{-1}))$, and conductance p.u.l. from zero to G_s as frequency increases from zero to infinity.

Likewise, the series inductance and resistance values are also functions of frequency which are sensitive to σ_{sub}. If analyzed at the two extreme values of σ_{sub}, zero and ∞, the inductance p.u.l. of the microstrip structure will be equivalent to that of a microstrip with insulating substrate of height $h_{ox}+h_{sub}$ or h_{ox}, respectively. The parameter σ_{sub} determines the frequency range where the transition between these two extremes occurs, since the skin depth, δ, is inversely proportional to σ_{sub} and frequency. The resistance p.u.l. of the Si-SiO_2 microstrip structure is an increasing function of frequency for a given σ_{sub}, as shown in Figs. 3.2 and 3.3, which show an increase in current crowding in the substrate with increasing frequency. However, for a given geometry and frequency, the resistance p.u.l. is not directly

proportional to σ_{sub}. This can be deduced from the fact that at the two extrema, $\sigma_{sub} = 0$ and ∞, the resistance p.u.l. is zero.

Clearly, a simple relationship between f_{sr}, Q_{max} and σ_{sub} does not exist, owing to the mechanisms described above. As shown in Figs. 3.3 and 3.2, the increase in f_{sr} for very high σ_{sub} is due to the reduction in inductance caused by the current crowding at the oxide/Si interface since f_{sr} is proportional to $1/\sqrt{LC}$. However, the peak Q occurs for a relatively low value of σ_{sub}, indicating that even though series losses due to substrate effects eventually decline with increasing σ_{sub} for a given frequency, the reduced inductances are significant enough to lower Q_{max}.

4.2. Simulation/Measurement Results

4.2.1. Simulation Results for MIS Example Structure

To examine the accuracy of the methodology for modeling MIS structures presented in Chapter Three, the example structure used in the study of the line constants was simulated for two different lower substrate conductivities using HP Momentum, a commercial planar structure electromagnetic simulator. Figures 4.3 and 4.4 show a comparison of c, g, r, and l as functions of frequency. The results are in very good agreement, which reinforces the validity of the modeling techniques presented in Chapter Three.

4.2.2. Spiral Model Validation

As an example of a structure with relatively low substrate conductivity, a 5 nH spiral from [2] with $\sigma_{\mathrm{Si}} = 10$ S/m is simulated using a model which does not

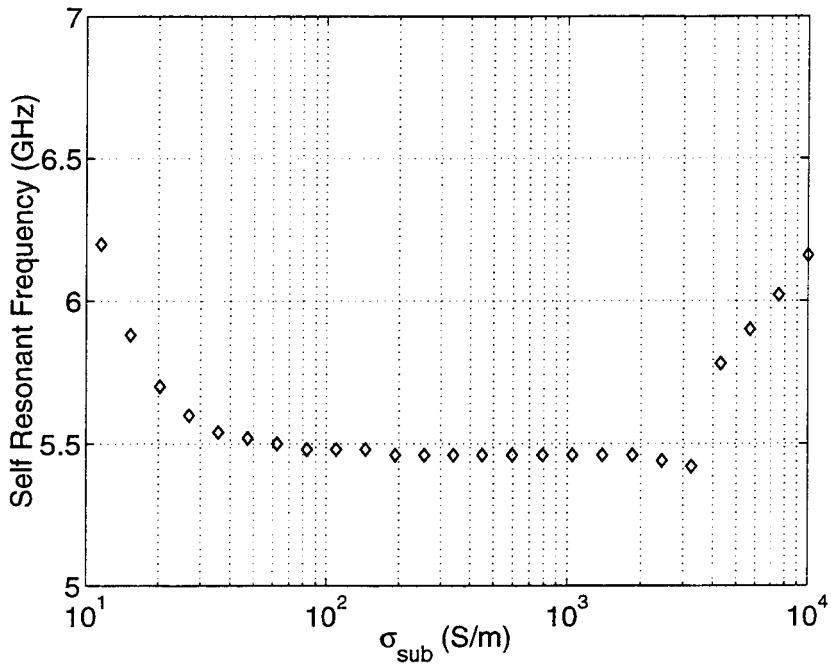

(a)

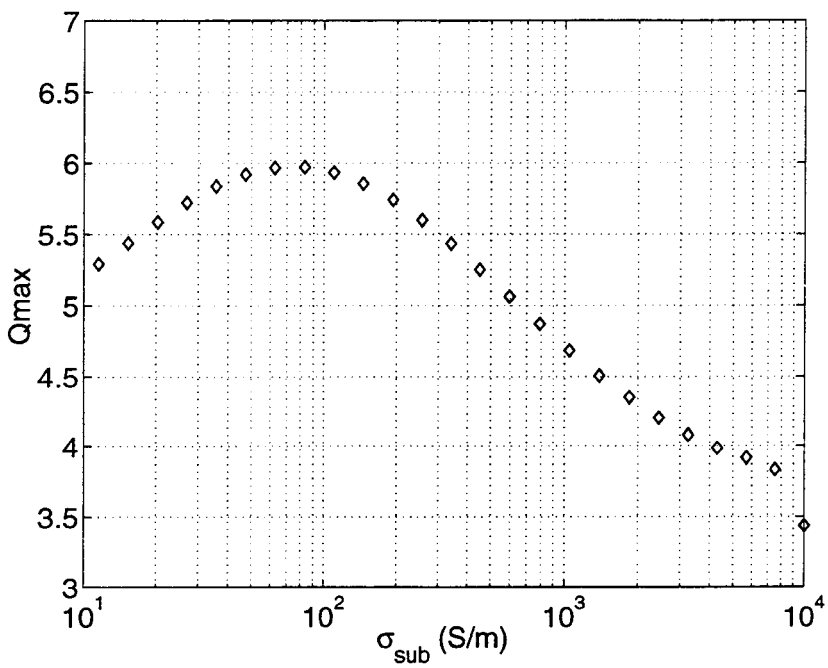

(b)

FIGURE 4.2. (a) f_{sr} and (b) Q_{max} for a 4.5 turn SLS vs. σ_{sub} ($h_{sub} = 120\mu$m, $h_{ox} = 4\mu$m)

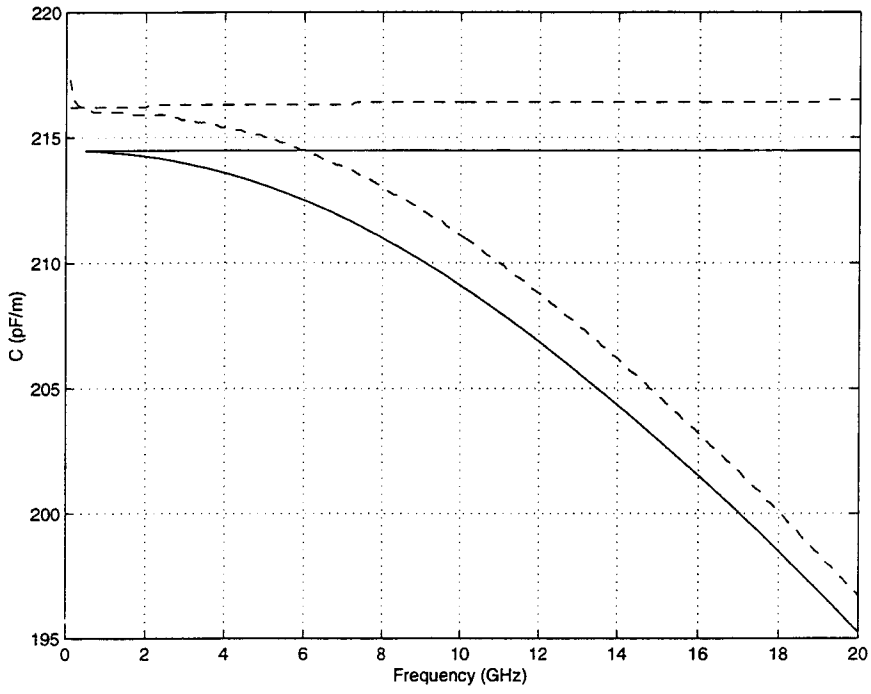

(a)

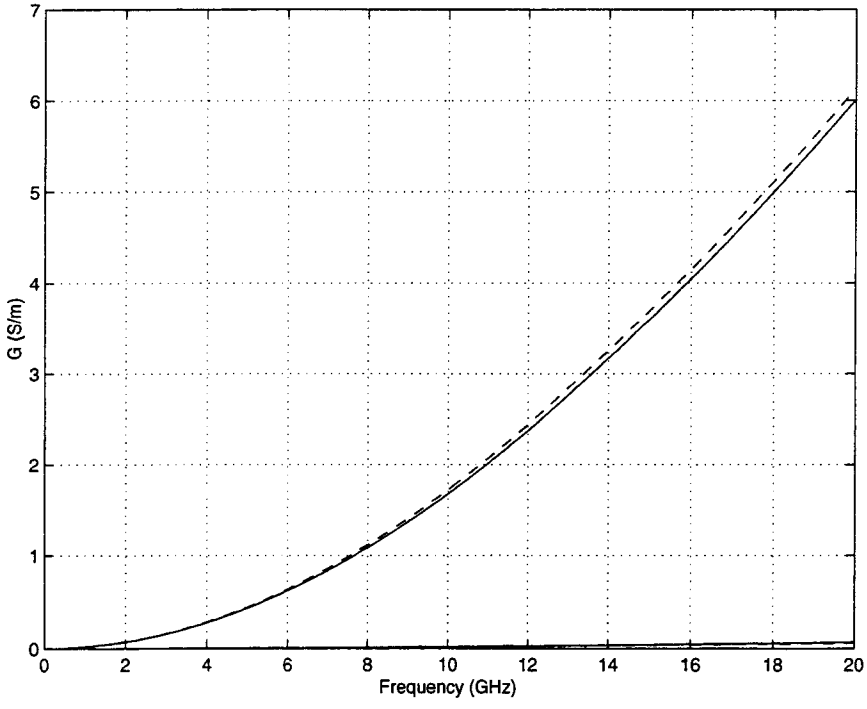

(b)

FIGURE 4.3. a) Capacitance (σ = 100 (lower lines), 10,000 (upper lines) S/m) and b) conductance (σ = 100 (upper lines), 10,000 (lower lines) S/m) p.u.l. as functions of frequency (- - Momentum, – Model developed in this thesis)

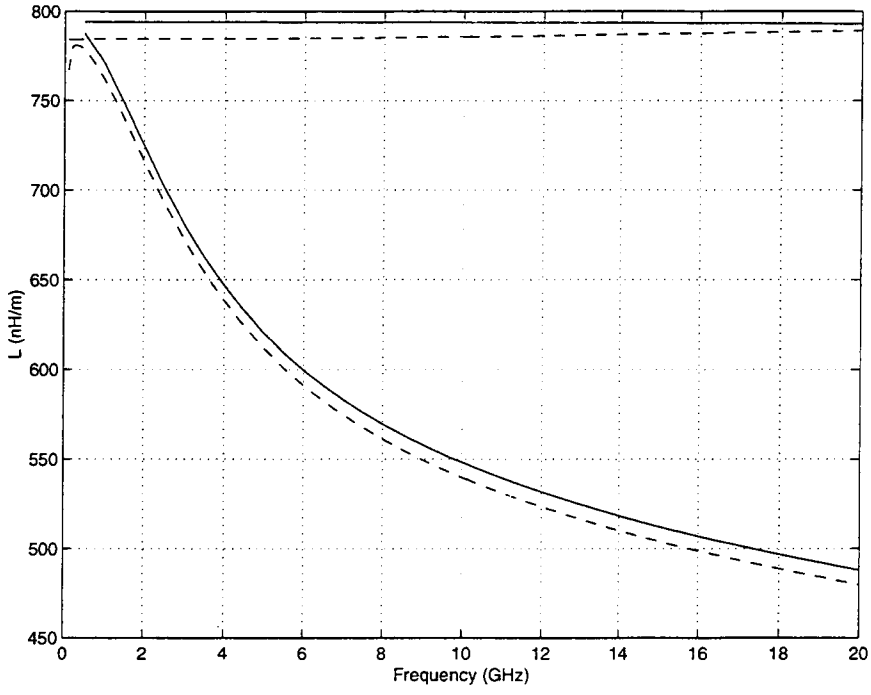

(a)

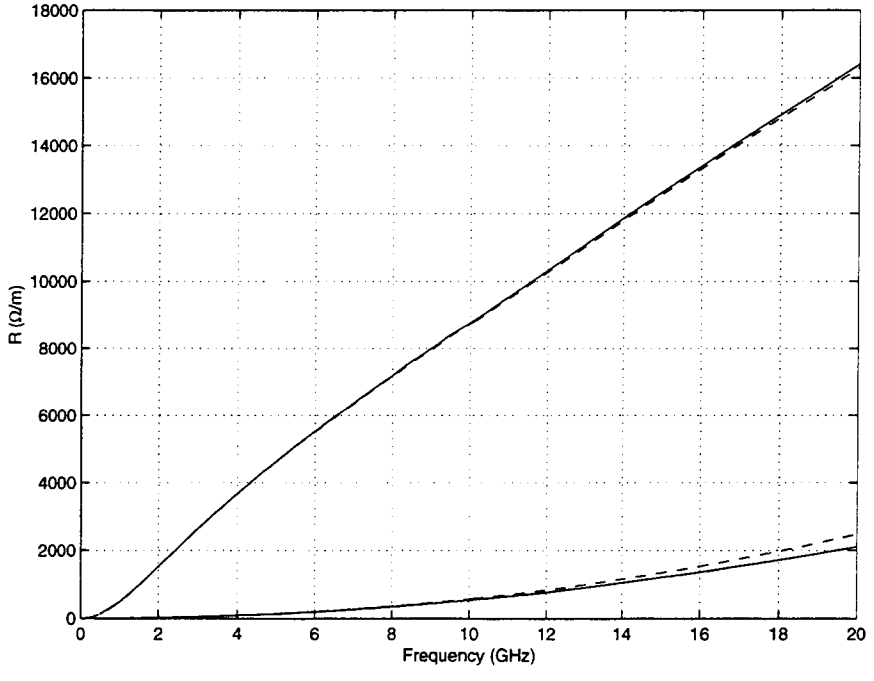

(b)

FIGURE 4.4. a) Inductance (σ = 100 (upper lines), 10,000 (lower lines) S/m) and b) resistance (σ = 100 (lower lines), 10,000 (upper lines) S/m) p.u.l. as functions of frequency (- - Momentum, – Model developed in this thesis)

address the skin effect mode. The results are adequate for this particular structure, as can be observed in Fig. 4.5.

Next, we consider a 9.5 turn, 10 nH spiral fabricated in CMOS technology with $\sigma_{Si} = 10^4$ S/m. Fig. 4.6 shows a comparison of three models with measured data. The proposed distributed model and corresponding ladder network (Fig. 3.16) properly account for the skin effect mode, in contrast to the model that only includes shunt conductances to represent the substrate losses. It is clear that the inclusion of the substrate skin effect is necessary for accurate modeling of the structure. In addition, it is observed that the ladder network approximation yields a response virtually identical to the distributed model for frequencies from dc to near the first resonance.

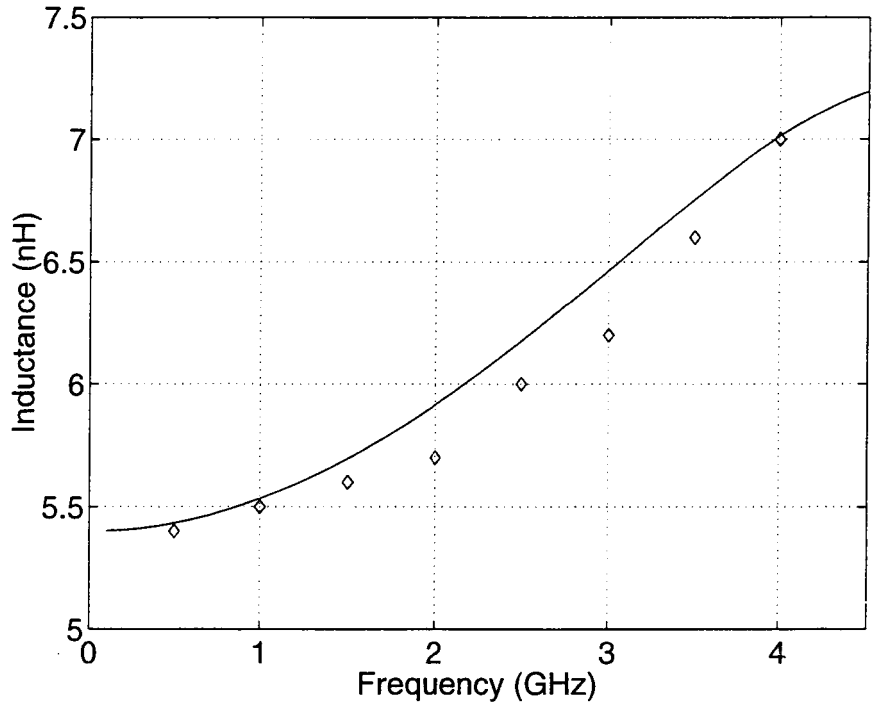

(a)

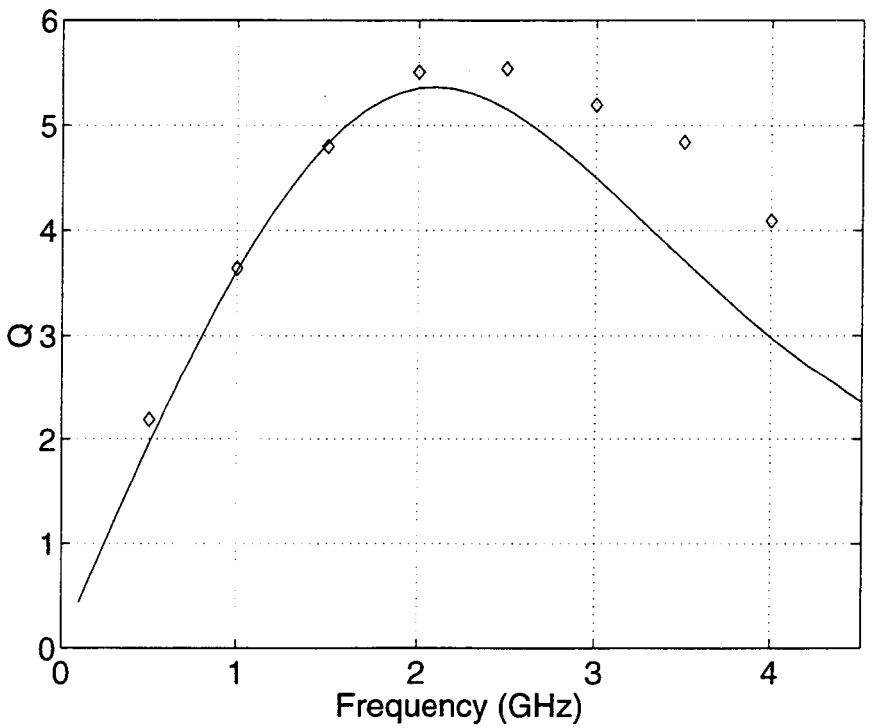

(b)

FIGURE 4.5. Comparison of (a) inductance and (b) quality factor for simulations without Si substrate effects (–) versus measured data (◇) for a 5 nH spiral with $\sigma_{sub} = 10$ S/m

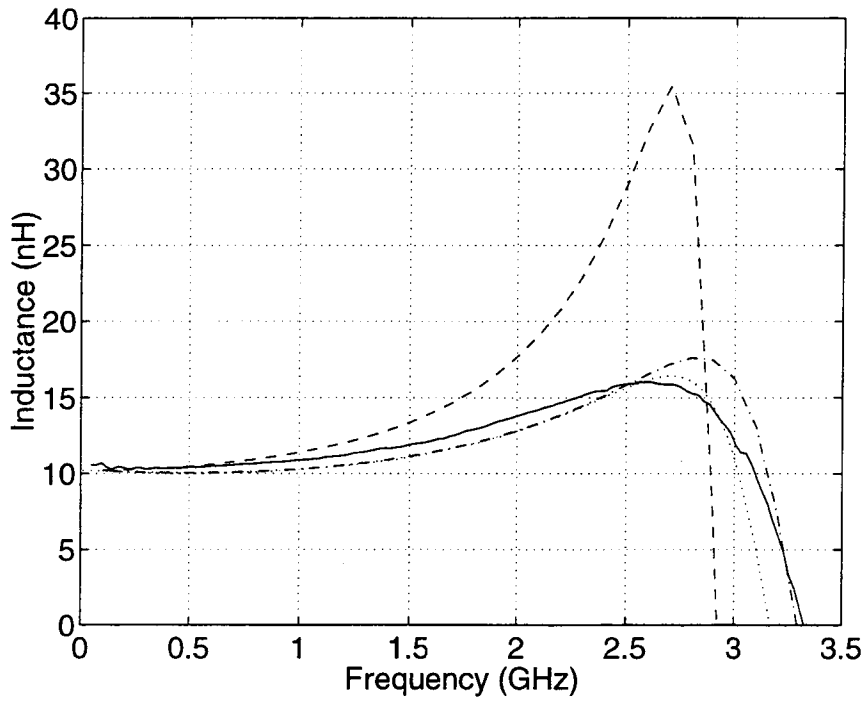

(a)

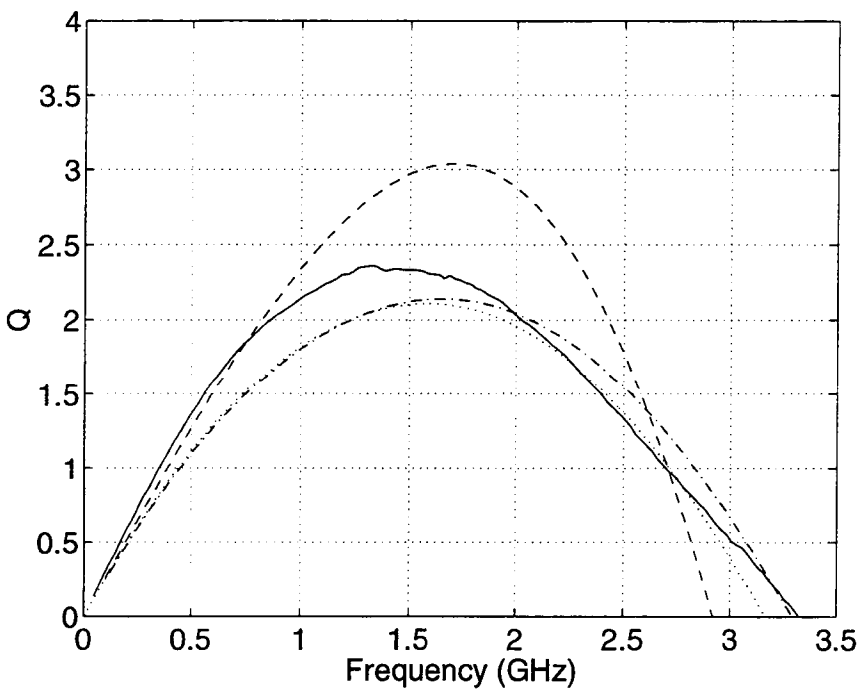

(b)

FIGURE 4.6. Comparison of (a) inductance and (b) quality factor for simulations with (-·· distributed, ·· ladder) and without (- -) Si substrate effects, versus measured data (–)

5. CONCLUSION

This thesis has presented methods for the analysis, modeling, and design of spiral inductors fabricated in lossy media such as CMOS and bipolar processes. In Chapter Two it was demonstrated that CAD-oriented modeling techniques may be used to simulate the performance of spiral inductors in low-loss multilayered media. The design methodology presented has been validated by experimental VNA measurement. Inductor parameters such as usable frequency range, near and far field coupling estimates, and quality factor are extractable from these models, which can be used in the design of RF or mixed signal modules. Chapter Three introduced the frequency dependent behavior of microstrip in lossy media, such as in Si-SiO_2-based systems, and demonstrated that this behavior necessitates line and spiral inductor models which include the skin effect mode at RF frequencies. In Chapter Four, it was shown that the proposed model for spiral inductors on lossy substrates is in better agreement with measured data for higher conductivity-frequency products ($\sigma\omega$'s) than previous models which only address transverse currents. It is seen that the skin-effect mode in particular must be considered for accurate analysis and modeling of spiral inductors fabricated on lossy substrates as in CMOS technology.

The techniques presented in this dissertation are applicable to CAD implementations in terms of equivalent circuit models. It has been shown that the frequency dependences of the capacitances and conductances found via the SDA using complex dielectric constants may be accurately represented by a novel fixed lumped element circuit topology which corresponds to the physical characteristics of the structure. Likewise, skin effect resistance in conductors may also be represented by an R-L ladder network, as presented in [17], if desired. To properly model the frequency dependences of the inductive elements, a virtual ground plane model has

been employed which currently is the only portion of the spiral model which is not represented by fixed lumped elements.

Future work in this area should include, but is not limited to, accurate modeling techniques for additional components of spiral designs such as substrate contacts and their associated currents, as well as multilevel spiral inductor and transformer designs in a lossy substrate environment. For the models presented here, it has been assumed that the substrate contact, if any, consists of a perfect conducting via which connects the substrate to ground at one end of the spiral. When the contact position is varied, or multiple contacts are used, there are additional currents in the substrate between the contacts and ground. Multilevel spiral designs in a lossy substrate environment introduce an additional design consideration with regard to the minimization of losses, and the modeling techniques presented here lend themselves well to being extended to such designs.

BIBLIOGRAPHY

[1] E. Pettenpaul *et al.*, "CAD Models of Lumped Elements on GaAs up to 18 GHz," *IEEE Trans. Microwave Theory Tech.*, pp. 294-304, Vol. 36, Feb. 1988.

[2] J. R. Long and M. A. Copeland, "The Modeling, Characterization, and Design of Monolithic Inductors for Silicon RF IC's," *IEEE J. Solid State Circuits*, Vol. 32, No. 3, pp. 357-369, Mar. 1997.

[3] H.M. Greenhouse, "Design of Planar Rectangular Microelectronic Inductors," *IEEE Trans. Parts, Hybrids, and Packaging*, Vol. PHP-10, pp. 101-109, June 1974.

[4] H. Hasegawa, *et al.*, "Properties of Microstrip Line on Si-SiO_2 System," *IEEE Trans. Microwave Theory Tech.*, Vol. MTT19, pp. 869-881, Nov. 1971.

[5] J. P. K. Gilb and C. A. Balanis, "MIS Slow-Wave Structures Over a Wide Range of Parameters," *IEEE Trans. Microwave Theory Tech.*, pp. 2148-2154, Vol. 40, No. 12, Dec. 1992.

[6] E. Grotelüschen, L. S. Dutta, and S. Zaage, "Full-wave analysis and analytical formulas for the line parameters of transmission line on semiconductor substrates," *INTEGRATION, VLSI J.*, vol. 16, pp. 33-58, 1993.

[7] V.K. Tripathi, C. Holmes, M. Cochrane, and B. Allen, "A distributed CAD model for microstrip spiral inductors," *European Microwave Conference Digest*, pp. 723-724, September 1993.

[8] Y. Seo and V.K. Tripathi, "Spiral Inductors in RFIC's and MMIC's," *1995 Asia Pacific Microwave Conference Proc.*, Taejon, Korea, pp. 454-457, October 1995.

[9] A. Hill and V.K. Tripathi, "Analysis and Modelling of Coupled Microstrip Bend Discontinuities," *IEEE Int. Microwave Sym.*, pp. 1143-1146, June 1989.

[10] A. Hill and V.K. Tripathi, "An Efficient Algorithm for the 3D Analysis of Passive Microstrip Components and Discontinuties for Microwave and Millimeter Wave Circuits, " *IEEE Trans. Microwave Theory and Tech.* , Vol. 41, pp. 83-91, Jan. 1991.

[11] R. L. Remke and G. A. Burdick, "Spiral Inductors for Hybrid and Microwave Applications," *Proc. 24th Electron Components Conf.*, Washington, D.C., pp. 152-161, May 1974.

[12] J. Müller *et al.*, "RF-Design Considerations for Passive Elements in LTCC Material Systems," *Intl. Journal Microcircuits and Electronic Packaging*, Vol. 18, pp. 200-206, 1995.

[13] V.K. Tripathi and N. Orhanovic, "Time-Domain Characterization and Analysis of Dispersive Dissipative Interconnects," *IEEE Trans. Circuits and Systems*, Vol. 39, pp. 938-945, November 1992.

[14] J. N. Burghartz, M. Soyuer, and K. A. Jenkins, "Microwave Inductors and Capacitors in Standard Multilevel Interconnect Silicon Technology," *IEEE Trans. Microwave Theory Tech.*, Vol. MTT-44, pp. 100-104, Jan. 1996.

[15] J. Lin *et al.*, "Accurate Design of Inductors on Multi-Chip Module using High-Resistivity Silicon Substrate," *Proc. IEEE 1996 Mtg. EPEP*, pp. 187-189, October 1996.

[16] J. Y.-C. Chang, A. Abidi, and M. Gaitan, "Large Suspended Inductors on Silicon and Their Use in a 2-μm CMOS RF Amplifier," *IEEE Electron Device Letters*, Vol. 14, No. 5, pp. 246-248, May 1993.

[17] H. A. Wheeler, "Formulas for the skin effect," *Proc. IRE*, vol. 30, Sept. 1942, pp. 412-424.

[18] R. T. Kollipara and V. K. Tripathi, "Spectral Domain Analysis of Multiconductor Structures with Rectangular and Trapezoidal Cross Sections," *Microwave and Optics Letters*, John Wiley, Jan. 1990.

[19] A. E. Ruehli, "Equivalent Circuit Models for Three-Dimensional Multiconductor Systems" *IEEE Trans. Microwave Theory Tech.*, Vol. MTT-22, pp. 216-221, Mar. 1974.

[20] C. Hoer, C. Love, "Exact Inductance Equations for Rectangular Conductors with Applications to More Complicated Geometries," *J. of Research, Natl. Bureau Standards*, Vol. 69C, No. 2, pp. 127-137, Apr.-Jun. 1965.

[21] A. E. Ruehli, "Efficient Capacitance Calculations for Three-dimensional Multiconductor Systems," *IEEE Trans. Microwave Theory Tech.*, Vol. MTT-21, pp. 76-82, Feb. 1973.

[22] A. E. Ruehli and E. Chiprout, "The Importance of Retardation in PEEC Models for Electrical Interconnect and Package (EIP) Applications," *Proc. IEEE EPEP*, pp. 232-234, Oct. 1995.

[23] V. K. Tripathi, *et al.*, "Quasi TEM Spectral Domain Analysis of Thick Microstrips for Microwave and Digital Integrated Circuits," *Electronics Letters*, pp. 1138-1139, Aug. 1989.

[24] R. T. Kollipara and V. K. Tripathi, "An Efficient Spectral Domain Method for the Dispersion Characteristics of Moderately Thick Microstrip Lines," *IEEE Microwave and Guided Wave Letters*, pp. 100-101, Mar. 1992.

[25] K. B. Ashby, *et al.*, "High Q Inductors for Wireless Applications in a Complementary Silicon Process," *1994 Bipolar/BiCMOS Circuits Tech. Mtg.* pp. 179-182, 1994.

[26] R. D. Lutz, *et al.*, "Spiral Inductor Design Issues in a Multilayered Medium," *Proc. ISHM Intl. Microelectronics Sym.*, Oct. 1996.

[27] D. Krafesik, D. Dawson, "A Closed-form Expression for Representing the Distributed Nature of the Spiral Inductor," *1986 IEEE MTT Monolithic Circuits Sym. Digest*, pp. 87-91.

[28] E. Frian, *et al.*, "Computer Aided Design of Square Spiral Transformers and Inductors, *1989 IEEE Int. Microwave Sym.*, pp. 661-664.

[29] D. Lovelace, N. Camilleri, G. Kannell, "Silicon MMIC Inductor Modeling for High Volume Low Cost Applications," *Microwave Journal*, pp. 60-71, Aug. 1994.

APPENDICES

APPENDIX A. Theory of Partial Inductance

For an arbitrary conductor of constant cross-section, a_j, around a loop, the magnetic vector potential at a point r_i generated by a current I_j in a loop j may be calculated as,

$$\mathbf{A}_{ij} = \frac{\mu}{4\pi} \cdot \frac{I_j}{a_j} \oint_j \int_{a_j} \frac{d\mathbf{l}_j da_j}{r_{ij}} \tag{A1}$$

where $r_{ij} = |\mathbf{r}_i - \mathbf{r}_j|$ and $d\mathbf{l}_j$ is taken along the length of the conductor perpendicular to the cross-section. The assumption made here is that the current density perpendicular to the cross section is uniform. The flux linked by loop i can be calculated from the above expression as,

$$\psi_{ij} = \oint_i \int_{a_i} \mathbf{A}_{ij} \cdot d\mathbf{l}_i da_i \tag{A2}$$

where a_i is the constant cross section of conductor loop i. To calculate the mutual inductance

$$L_{ij} = \frac{\psi_{ij}}{I_j} \tag{A3}$$

between loops i and j using (A1) and (A2), the expressions for vector potential and flux linkage are inserted with the result being,

$$L_{ij} = \frac{1}{a_i a_j} \cdot \frac{\mu}{4\pi} \oint_i \int_{a_i} \oint_j \int_{a_j} \frac{d\mathbf{l}_i \cdot d\mathbf{l}_j}{r_{ij}} da_i da_j. \tag{A4}$$

This result is similar to the Neumann formula for mutual inductance between two arbitrary filaments of current,

$$L_{fij} = \frac{\mu}{4\pi} \oint_i \oint_j \frac{d\mathbf{l}_i d\mathbf{l}_j}{r_{ij}} \tag{A5}$$

where the subscript f stands for filament. In fact (A4) and (A5) are identical when the cross-sectional areas $a_{i,j}$ are zero. It is apparent averages are being taken in

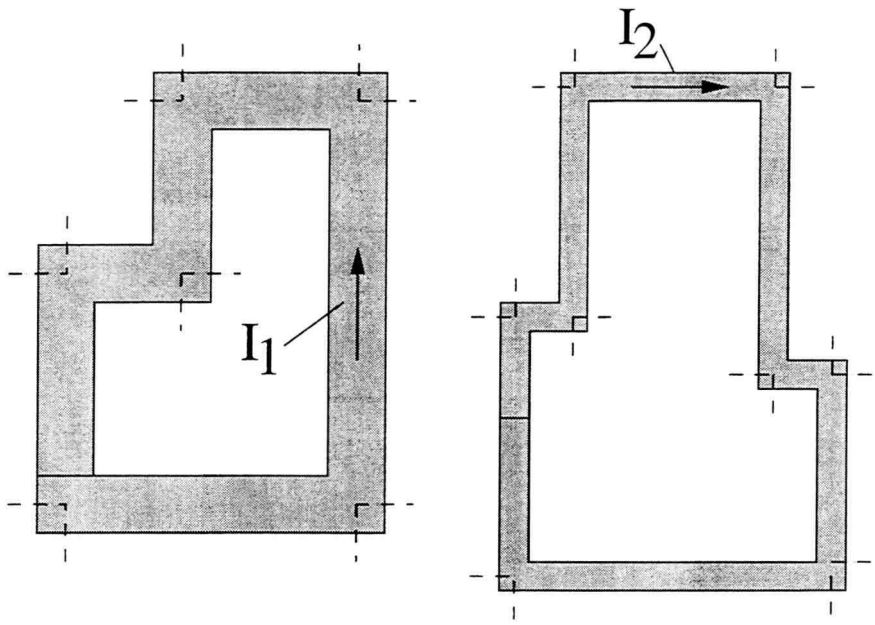

FIGURE 5.1. Example of two loops to be analyzed in terms of straight line sections

both (A1) and (A2), as both expressions are divided by the cross-sectional area of the conductor involved. Equation (A4) may be combined with (A5) to yield

$$L_{ij} = \frac{1}{a_i a_j} \int_{a_i} \int_{a_j} L_{fij} da_i da_j. \tag{A6}$$

If the conductors forming two loops are analyzed in terms of their respective straight line sections, as shown in Figure 5.1, the total inductance may be written in terms of a double summation as,

$$L_{km} = \sum_{k=1}^{K} \sum_{m=1}^{M} L_{p_{km}}. \tag{A7}$$

Here the term L_p is introduced to represent the partial mutual or self inductance of the respective conductor sections. The partial inductance for two straight conductors of constant cross sections is calculated using (A4) with the loop integrals replaced by line integrals,

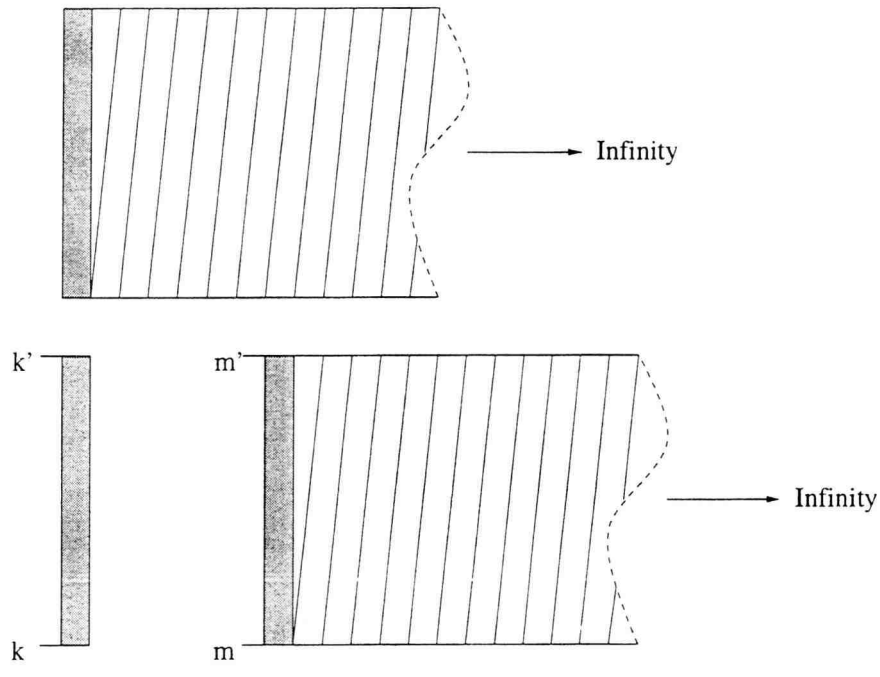

FIGURE 5.2. Flux linkage areas associated with self and mutual inductance calculations

$$L_{p_{km}} = \frac{1}{a_k a_m} \cdot \frac{\mu}{4\pi} \int_{a_k} \int_{a_m} \int_{k}^{k'} \int_{m}^{m'} \frac{d\mathbf{l}_k \cdot d\mathbf{l}_m}{r_{km}} da_k da_m. \tag{A8}$$

The direction of $d\mathbf{l}_{k,m}$ should be in accordance with the assumed current polarity in the loops which will lead to both positive and negative mutual inductances. To verify this approach, the flux linkage associated with each term in (A7) should be considered. For a partial self inductance term ($k = m$), the region of flux linkage extends from the conductor out to infinity. Likewise, for two conductors k and m, the flux linkage area for partial mutual inductance computations extends from the outside edge of one of the conductors $m(k)$ out to infinity and is also bounded on the edges by lines perpendicular to conductor $k(m)$ and extending from the end points of conductor $m(k)$. These two flux linkage areas are illustrated in Figure 5.2. If a

square loop is analyzed purely in terms of flux linkage, we may do the computation with a single surface integral,

$$L_{sq} = \frac{1}{I} \int_S \mathbf{B} \cdot d\mathbf{S}. \tag{A9}$$

Likewise, if two parallel conductors of the square loop are analyzed in terms of the flux linkages associated with the self and mutual inductances, it can be deduced that the net area will be that of the square itself (S in (A9)). This is clear upon observation that the flux linkage areas associated with the self inductance terms extend from the conductor to infinity, whereas the area of linkage associated with the mutual terms extends from the conductor of opposing current polarity out to infinity. The difference between these two areas is in fact the area inside the square loop.

APPENDIX B. Expressions for Quasi-Static Magnetic Vector Potential

To develop the fundamental equations used in the quasi-static calculation of the magnetic vector potential for an MIS structure, the magnetic field curl expression is used as a starting point,

$$\nabla \times \mathbf{H} = \mathbf{J} + \frac{\partial \mathbf{D}}{\partial t}. \tag{B1}$$

If the magnetic vector potential curl equation

$$\mu \mathbf{H} = \nabla \times \mathbf{A} \tag{B2}$$

is substituted for $\mathbf{H}$ in (B1), we obtain

$$\nabla \times \nabla \times \mathbf{A} = \mu \cdot \left[\mathbf{J} + \frac{\partial \mathbf{D}}{\partial t} \right] \tag{B3}$$

which may subsequently be rewritten as,

$$\nabla(\nabla \cdot \mathbf{A}) - \nabla^2 \mathbf{A} = \mu \cdot \left[\mathbf{J} + \frac{\partial \mathbf{D}}{\partial t} \right]. \tag{B4}$$

If the divergence of $\mathbf{A}$ is chosen such that,

$$\nabla \cdot \mathbf{A} = 0, \tag{B5}$$

which is known as the Coulomb gauge, and displacement current is neglected, then (B4) becomes,

$$\nabla^2 \mathbf{A} = -\mu \mathbf{J}. \tag{B6}$$

$\mathbf{J}$ may be rewritten in terms of $\mathbf{E}$ as,

$$\mathbf{J} = \sigma \mathbf{E}. \tag{B7}$$

Now, if we recall the curl equations for $\mathbf{E}$ and $\mathbf{A}$,

$$\nabla \times \mathbf{E} = -\frac{\partial \mathbf{B}}{\partial t} \tag{B8}$$

$$\nabla \times \mathbf{A} = \mathbf{B}, \tag{B9}$$

we can write,

$$\nabla \times \mathbf{E} = -\frac{\partial}{\partial t} \nabla \times \mathbf{A} \tag{B10}$$

$$\mathbf{E} = -\frac{\partial}{\partial t} \mathbf{A} \tag{B11}$$

Assuming a sinusoidal steady-state solution is desired, we may express $\mathbf{J}$ as

$$\mathbf{J} = -j\omega\sigma\mathbf{A} \tag{B12}$$

which leads us to the final form for (B6) given in Chapter Three,

$$\nabla^2 \mathbf{A} = j\omega\mu\sigma\mathbf{A}. \tag{B13}$$

The solutions for A_z for the different regions of a Si-SiO_2 based microstrip structure in the spatial domain (to be given below) are based on the expressions derived in [6] for coplanar structures with no ground plane. Here it is assumed that current only exists along the direction of propagation, the z-coordinate for this case, and thus $\mathbf{A}$ will only consist of a single component A_z. This allows for a solution of a two dimensional scalar potential problem which simplifies the analysis.

For the non-conducting regions (i.e. air and oxide layers), the z-directed magnetic vector potential must satisfy

$$\nabla^2 A_z(x, y) = 0, \tag{B14}$$

while for conducting regions (i.e. bulk Si substrate),

$$\nabla^2 A_z(x, y) = j\omega\mu\sigma A_z(x, y). \tag{B15}$$

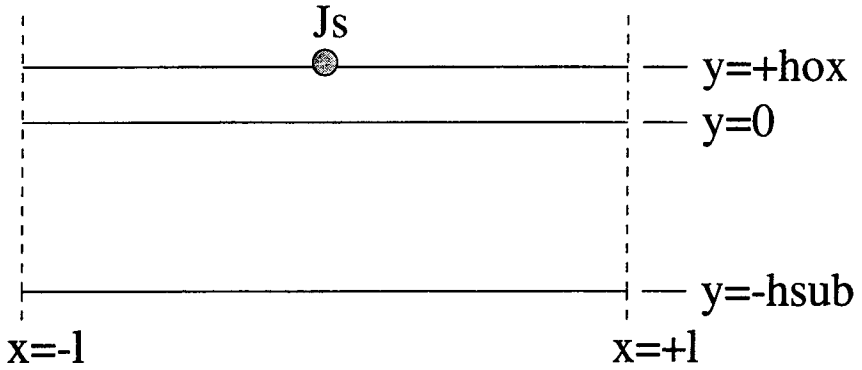

FIGURE 5.3. Structure used for solution of magnetic potential

Assuming a line current at $x = 0$ and $y = h_{ox}$, the solutions for A_z in both conducting and nonconducting regions are found by applying appropriate boundary conditions,

$$A_z(x, y = -h_{sub}) = 0 \tag{B16}$$

$$\frac{dA_z(x = \pm l, y)}{dx} = 0 \tag{B17}$$

where $\pm l$ are the locations of two symmetric magnetic walls, shown in Figure 5.3, which are introduced to simplify the solutions in terms of Fourier series. The solutions in the two regions are

$$A_z(x, y \geq 0) = \frac{\mu_o I}{2\pi} \ln \sqrt{\frac{x^2 + (y + h_{ox})^2}{x^2 + (y - h_{ox})^2}} + \frac{\mu_o I}{l} \left[\frac{E_0}{2} + \sum_{k=1}^{\infty} E_k cos(m_k x) \right] \tag{B18}$$

$$A_z(x, y \leq 0) = \frac{\mu_o I}{l} \left[\sum_{k=1}^{\infty} 2m_k \sinh(q_k(y + h_{sub})) e^{-m_k h_{ox}} cos(m_k x) \right] \tag{B19}$$

where

$$E_k = \frac{q_k \cosh(2q_k h_{sub}) + m_k \sinh(2q_k h_{sub}) - 2q_k}{(q_k^2 + m_k^2)\sinh(2q_k h_{sub}) + 2q_k m_k \cosh(2q_k h_{sub})} \cdot e^{-2m_k h_{ox}} \tag{B20}$$

$$m_k = \frac{k\pi}{l} \tag{B21}$$

$$q_k = \sqrt{m_k^2 + j\omega\mu\sigma} \tag{B22}$$

The infinite summations in (B18) and (B19) are Fourier series representations of the continuous integrals involved when there are no magnetic walls present.